JOURNAL OF PETROLOGY | VOLUME 46 | NUMBER 3 | PAGES 641–669 | 2005 | doi:10.1093/petrology/egh092

Exhumation Paths of High-Pressure–Low-Temperature Metamorphic Rocks from the Lycian Nappes and the Menderes Massif (SW Turkey): a Multi-Equilibrium Approach

GAËTAN RIMMELÉ[1,2]*, TEDDY PARRA[1], BRUNO GOFFÉ[1], ROLAND OBERHÄNSLI[2], LAURENT JOLIVET[3] AND OSMAN CANDAN[4]

[1]LABORATOIRE DE GÉOLOGIE DE L'ECOLE NORMALE SUPÉRIEURE, CNRS, UMR 8538, 24, RUE LHOMOND, 75005 PARIS, FRANCE

[2]INSTITUT FÜR GEOWISSENSCHAFTEN, UNIVERSITÄT POTSDAM, KARL LIEBKNECHTSTRASSE 24–25, D-14476 POTSDAM-GOLM, GERMANY

[3]LABORATOIRE DE TECTONIQUE, UMR 7072, UNIVERSITÉ PIERRE ET MARIE CURIE, TOUR 26-0, ETAGE 1, CASE 129, 4, PLACE JUSSIEU, 75252 PARIS CEDEX 05, FRANCE

[4]DOKUZ EYLÜL ÜNIVERSITESI, MÜHENDISLIK-MIRMALIK FAKÜLTESI, JEOLOJI MÜH. BÖLÜMÜ, TR-35100 BORNOVA–IZMIR, TURKEY

RECEIVED NOVEMBER 15, 2003; ACCEPTED OCTOBER 21, 2004
ADVANCE ACCESS PUBLICATION DECEMBER 14, 2004

The Menderes Massif and the overlying Lycian Nappes occupy an extensive area of SW Turkey where high-pressure–low-temperature metamorphic rocks occur. Precise retrograde P–T *paths reflecting the tectonic mechanisms responsible for the exhumation of these high-pressure–low-temperature rocks can be constrained with multi-equilibrium* P–T *estimates relying on local equilibria. Whereas a simple isothermal decompression is documented for the exhumation of high-pressure parageneses from the southern Menderes Massif, various* P–T *paths are observed in the overlying Karaova Formation of the Lycian Nappes. In the uppermost levels of this unit, far from the contact with the Menderes Massif, all* P–T *estimates depict cooling decompression paths. These high-pressure cooling paths are associated with top-to-the-NNE movements related to the Akçakaya shear zone, located at the top of the Karaova Formation. This zone of strain localization is a local intra-nappe contact that was active in the early stages of exhumation of the high-pressure rocks. In contrast, at the base of the Karaova Formation, along the contact with the Menderes Massif,* P–T *calculations show decompressional heating exhumation paths. These paths are associated with severe deformation characterized by top-to-the-east shearing related to a major shear zone (the Gerit shear zone) that reflects late exhumation of high-pressure parageneses under warmer conditions.*

KEY WORDS: *exhumation; high-pressure–low-temperature metamorphism; multi-equilibrium* P–T *estimates; Lycian Nappes; Menderes Massif*

INTRODUCTION

High-pressure–low-temperature (HP–LT) metamorphic rocks are widely exposed in the Alpine–Himalayan Belt. Plate tectonic processes can account for HP–LT metamorphism by fast burial during subduction and crustal thickening; however, the mechanisms responsible for the return of these metamorphic rocks to the surface are far less understood. Extensive metamorphic domains exposing rocks that recorded blueschist- to eclogite-facies conditions have been described in the Aegean region (Blake *et al.*, 1981; Mposkos & Perdikatsis, 1984; Okrusch *et al.*,

*Corresponding author. Telephone: 00 33 1 44 32 22 74. Fax: 00 33 1 44 32 20 00. E-mail: rimmele@geologie.ens.fr

1984; Okrusch & Bröcker, 1990; Mposkos & Liati, 1991; Theye & Seidel, 1991; Theye *et al.*, 1992; Forster & Lister, 1999). During the last decade, it has been emphasized that exhumation of these HP–LT rocks involves a significant role of major low-angle extensional shear zones (Avigad & Garfunkel, 1989; Gautier *et al.*, 1993; Gautier & Brun, 1994; Jolivet *et al.*, 1994, 1996; Jolivet & Patriat, 1999; Trotet, 2000; Trotet *et al.*, 2001*a*). Farther east, western Turkey preserves similar HP–LT metamorphism occurrences (Okay, 1984; Okay & Kelley, 1994; Candan *et al.*, 1997, 2001, 2002; Oberhänsli *et al.*, 1997, 1998, 2001; Çetinkaplan, 2002; Okay *et al.*, 2002; Rimmelé, 2003; Rimmelé *et al.*, 2003*a*, 2003*b*). In this region, the Menderes Massif occupies an extensive area; it is tectonically overlain by nappe units of the Izmir–Ankara Suture Zone (Şengör & Yilmaz, 1981) in the north (including the Bornova Flysch Zone) and the Lycian Nappes in the south (Brunn *et al.*, 1970; de Graciansky, 1972; Poisson, 1977; Collins & Robertson, 1998). The recent discovery of the HP–LT mineral Fe–Mg-carpholite within the Lycian Nappes (Oberhänsli *et al.*, 2001; Rimmelé *et al.*, 2003*a*) and the southern Menderes Massif (Rimmelé *et al.*, 2003*b*) has led to a revision of the tectono-metamorphic evolution of this region (Fig. 1). In the Lycian Nappes, the HP–LT rocks have been found widely on the Bodrum peninsula and locally in a few Lycian Nappe klippen located on top of the Menderes metamorphic rocks (on the Dilek peninsula, in the Çivril area, and close to the locality of Borlu; Fig. 1). In the Menderes Massif, the HP–LT rocks have been described in the southernmost part of the massif, north of the boundary between the Lycian Nappes and the Menderes Massif. Evidence of HP–LT metamorphism in both nappe complexes suggests significant burial, of at least 30 km, during nappe stacking (Oberhänsli *et al.*, 2001; Rimmelé, 2003; Rimmelé *et al.*, 2003*a*, 2003*b*; Jolivet *et al.*, 2004). In the Bodrum peninsula area, Rimmelé *et al.* (2003*a*) reported the existence of major shear zones that were active during exhumation of the HP–LT rocks. Structural data from the Bodrum peninsula region indicate top-to-the-NE to top-to-the-east senses of shear with intensification of deformation approaching the shear zones.

Whereas P–T conditions of the metamorphic peak for the Menderes HP–LT rocks (>10 kbar/>440°C; Rimmelé *et al.*, 2003*b*) and the Lycian HP–LT metasedimentary rocks (~8 kbar/<400°C; Oberhänsli *et al.*, 2001; Rimmelé *et al.*, 2003*a*) can easily be estimated from the composition of metamorphic index minerals (Fig. 1), detailed and precise retrograde P–T paths reflecting the tectonic mechanisms responsible for exhumation are rather difficult to constrain. However, recent studies have shown that in low- to medium-grade garnet-free metapelites, phengite and chlorite local equilibria are good candidates to constrain the retrograde P–T evolution of exhumed metamorphic rocks (Vidal & Parra, 2000). The method, which consists of multi-equilibrium P–T estimates relying on local equilibria, has recently been used to obtain a detailed picture of retrograde P–T paths for exhumed rocks in the Aegean domain (Trotet, 2000; Trotet *et al.*, 2001*b*; Parra *et al.*, 2002*b*). These studies distinguished a syn-orogenic exhumation stage (Eocene) characterized by a cold P–T path (decrease of temperature and pressure) during construction of the Hellenides, whereas the subsequent post-orogenic exhumation (Oligo-Miocene) occurred along a warmer P–T path (isothermal decompression) during formation of the Aegean Sea, a thermal re-equilibriation of the crust being envisaged between the two exhumation episodes (Parra *et al.*, 2002*b*).

In the present study, we use the multi-equilibrium calculation method to obtain precise information on the exhumation pattern of the Lycian and Menderes HP–LT rocks, and to try to relate the deformation with the intensity of retrogression in the high-pressure metapelites.

GEOLOGICAL SETTING OF THE MENDERES MASSIF AND THE LYCIAN NAPPES

The Menderes Massif

The Menderes Massif is split into three submassifs by Neogene grabens: the southern submassif (or Çine submassif), the central and the northern submassifs (Fig. 2). Traditionally the Menderes Massif has been stratigraphically subdivided into a gneissic core with an overlying metasedimentary cover (Schuiling, 1962; de Graciansky, 1966; Dürr, 1975; Şengör *et al.*, 1984; Satır & Friedrichsen, 1986). Recent studies have shown that this picture is oversimplified and that the Menderes Massif forms a thick-skinned nappe pile (Partzsch *et al.*, 1997; Hetzel *et al.*, 1998; Ring *et al.*, 1999*a*; Gessner, 2000; Gessner *et al.*, 2001*a*, 2001*b*) assembled during Late Cretaceous to Tertiary orogenesis.

Core rocks are composed of augen gneisses, migmatites, gabbros with some granulite and eclogite relics, and medium- to high-grade metamorphic schists (Şengör *et al.*, 1984; Satır & Friedrichsen, 1986; Oberhänsli *et al.*, 1997; Candan *et al.*, 2001). They form the basement of western Turkey and were deposited, intruded and metamorphosed in Neoproterozoic–Cambrian times (Schuiling, 1962; Şengör *et al.*, 1984; Satır & Friedrichsen, 1986; Konak *et al.*, 1987; Hetzel & Reischmann, 1996; Hetzel *et al.*, 1998; Loos & Reischmann, 1999; Gessner *et al.*, 2001*a*, 2004). In the central submassif, eclogite-facies metamorphism occurred (Oberhänsli *et al.*, 1997; Candan *et al.*, 2001) and was later overprinted by regional amphibolite-facies metamorphism (Candan *et al.*, 2001).

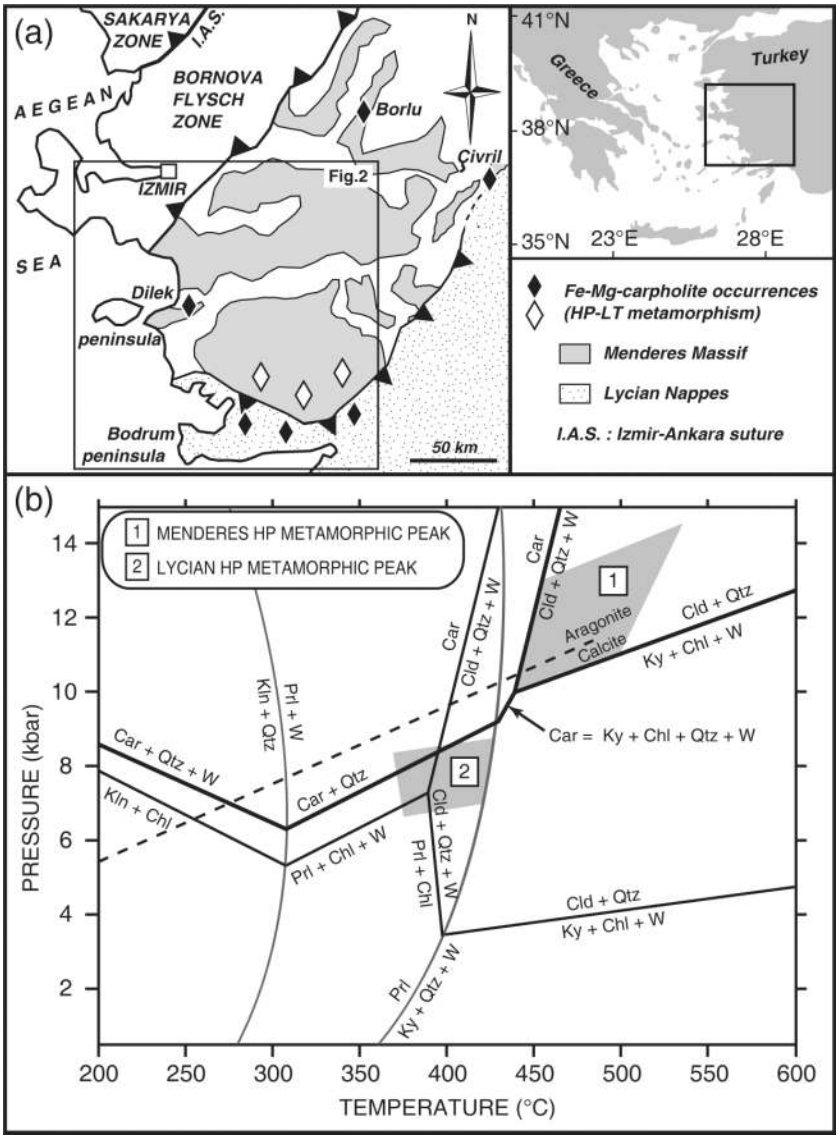

Fig. 1. (a) Simplified map showing the occurrences of Fe–Mg-carpholite-bearing rocks in SW Turkey. ◆, Fe–Mg-carpholite localities in the Lycian Nappes (*sensu stricto* and klippen; Oberhänsli *et al.*, 2001; Rimmelé *et al.*, 2003*a*); ◇, magnesiocarpholite occurrences in the Menderes Massif (Rimmelé *et al.*, 2003*b*). (b) *P–T* diagram showing location of metamorphic peak conditions estimated for parageneses involving Fe–Mg-carpholite in the Lycian Nappes and the Menderes Massif; each equilibrium curve involving carpholite, chloritoid and chlorite has been calculated with the mineral compositions measured in the Lycian Nappes (fine lines; Rimmelé *et al.*, 2003*a*) as well as in the Menderes Massif (bold lines; Rimmelé *et al.*, 2003*b*). W, water; Qtz, quartz; Car, Fe–Mg-carpholite; Cld, chloritoid; Chl, chlorite; Kln, kaolinite; Prl, pyrophyllite; Ky, kyanite.

This HP–LT metamorphism has been dated as Neoproterozoic–Cambrian (Pan-African) and is considered to result from crustal thickening during the Late Precambrian–Early Palaeozoic orogeny (Partzsch *et al.*, 1997; Candan *et al.*, 2001; Warkus, 2001; Oberhänsli *et al.*, 2002).

Cover rocks consist of a Palaeozoic schist envelope and a Mesozoic to Cenozoic marble envelope (Figs 2 and 3). The schist envelope is made of garnet-, kyanite-, staurolite-, chloritoid-, and sillimanite-bearing micaschists, graphite-rich quartzitic phyllite–schists, garnet amphibolites, and marble intercalations (Dürr, 1975; Akkök, 1983; Ashworth & Evirgen, 1984*a*; Şengör *et al.*, 1984; Satır & Friedrichsen, 1986; Konak *et al.*, 1987; Bozkurt, 1996; Hetzel *et al.*, 1998; Whitney & Bozkurt, 2002; Régnier *et al.*, 2003). The schist sequence is overlain by a thick marble envelope. An Upper Triassic conglomerate containing quartzite pebbles, yellowish dolomite, quartzite and fine-grained micaschist intercalations lies at the base of the marble series (Fig. 3). In this

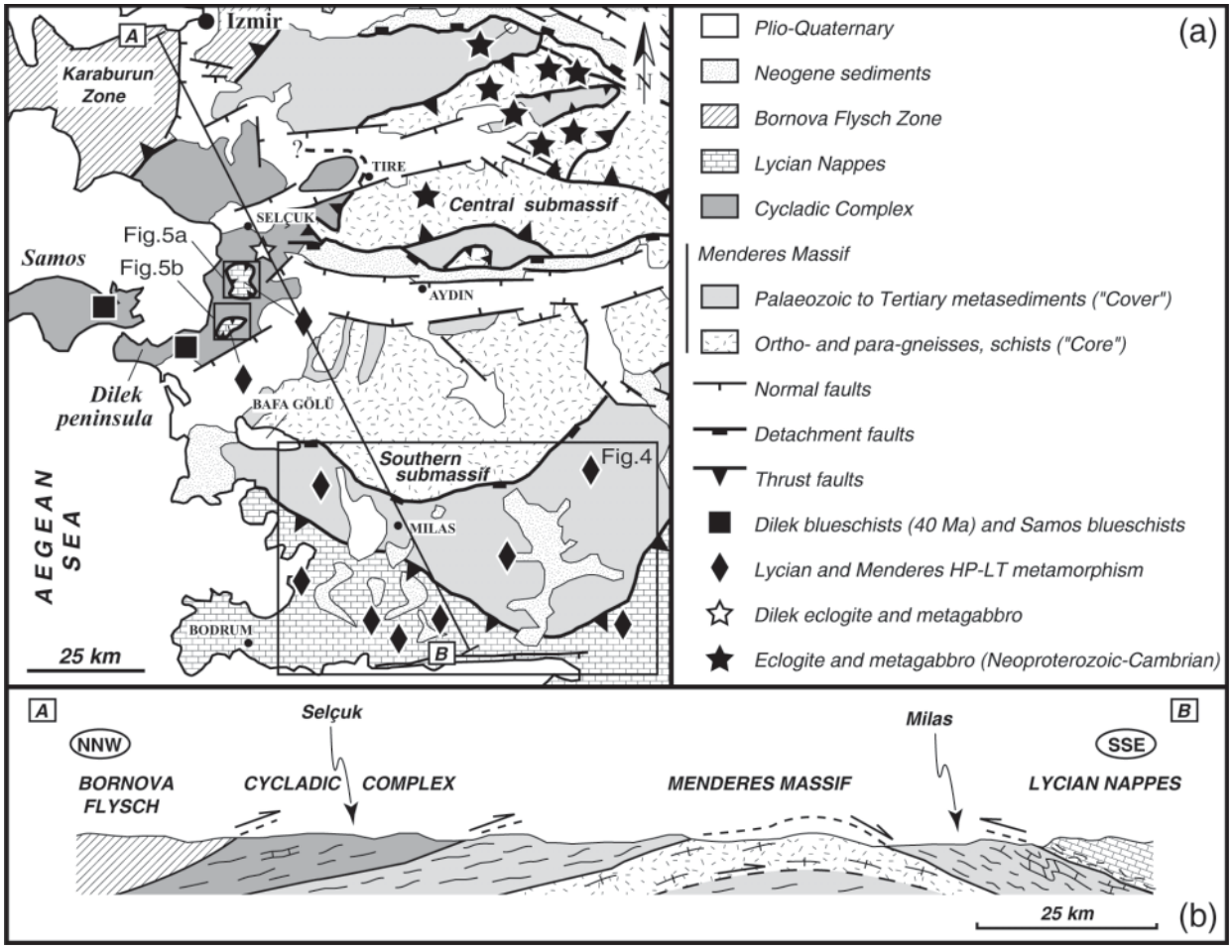

Fig. 2. (a) Geological map of the Menderes Massif and Lycian Nappes region showing the regional distribution of HP–LT rocks in SW Turkey [modified after Bozkurt & Satır (2000), Candan *et al.* (2001), Okay (2001) and Rimmelé *et al.* (2003*b*); see text for further references]. (b) Simplified cross-section across SW Turkey [modified after Jolivet *et al.* (2004)]. The recent shear zones and grabens are intentionally not represented.

formation that locally crops out in the southern submassif, magnesiocarpholite–kyanite–chloritoid assemblages have recently been discovered in quartz segregations appearing as synfolial veins, and led to the recognition of a HP–LT metamorphic event (Eocene?) that affected the Menderes Massif during its Alpine evolution (minimum 10–12 kbar/440°C; Rimmelé *et al.*, 2003*b*). The three localities where HP–LT parageneses have been found are shown in Fig. 4. Magnesiocarpholite is essentially retrogressed to chlorite and kyanite and the existence of corundum-bearing rocks in the overlying rocks suggests an isothermal decrease of pressure during exhumation of HP–LT metamorphic rocks (Rimmelé *et al.*, 2003*b*). This metamorphic formation is overlain by Upper Triassic to Liassic marbles, Jurassic to Lower Cretaceous massive dolomitic marbles with metabauxite containing corundum and diaspore (Konak *et al.*, 1987; Yalçin, 1987), Upper Cretaceous (Santonian–Campanian) rudist-bearing marbles (Dürr, 1975; Konak *et al.*, 1987; Özer, 1998; Özer *et al.*, 2001), and Upper Campanian–Upper Maastrichtian reddish pelagic cherty marbles (Konak *et al.*, 1987; Özer, 1998; Özer *et al.*, 2001). A Middle Palaeocene metamorphic olistostromal unit including metaserpentinite and marble blocks within a schist matrix unconformably overlies the marble sequence (Dürr, 1975; Gutnic *et al.*, 1979; Çağlayan *et al.*, 1980; Konak *et al.*, 1987; Collins & Robertson, 1998; Özer *et al.*, 2001; Collins & Robertson, 2003). This formation marks the end of sedimentation in the Menderes Massif.

In the southern submassif, this metaolistostromal unit has been described as slightly metamorphosed (Gutnic *et al.*, 1979; Rimmelé, 2003). In contrast, relics of eclogite and eclogitic metagabbro were found in blocks of an olistostromal unit ('Selçuk Formation'; Güngör & Erdoğan, 2001), near the locality of Selçuk, as described by Candan *et al.* (1997), Oberhänsli *et al.* (1998) and Çetinkaplan (2002) (Fig. 2). Those workers also suggested

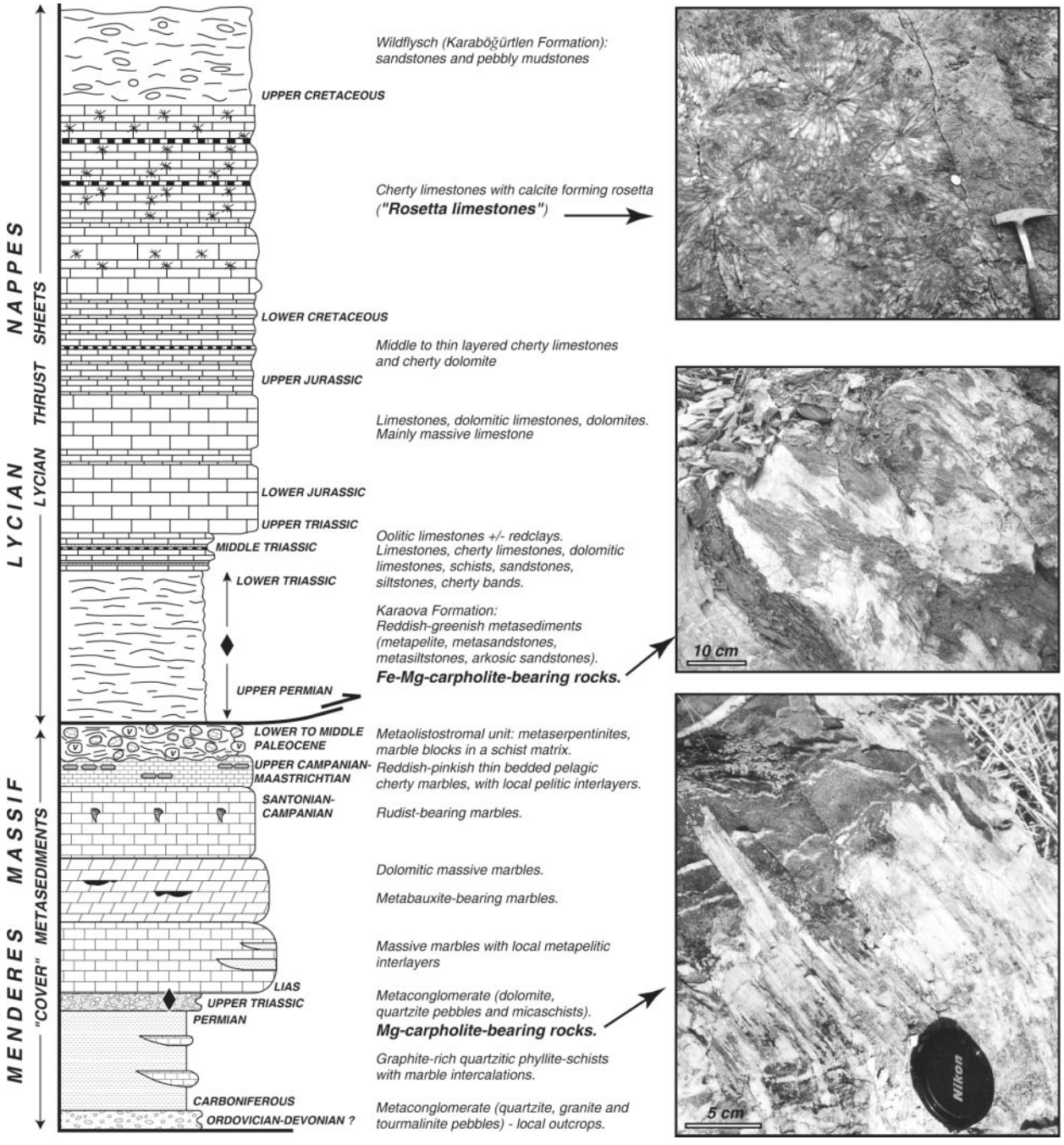

Fig. 3. Generalized stratigraphic section (section not to scale) of the Menderes metasedimentary 'cover' and the overlying Lycian Thrust Sheets [modified after Çakmakoğlu (1985), Dora *et al.* (2001), Özer *et al.* (2001) and Rimmelé *et al.* (2003*a*)]. Locations of HP–LT assemblages are indicated.

that the matrix of this olistostrome, which does not show any evidence of HP–LT metamorphism, has been completely overprinted by later greenschist-facies assemblages whereas the mafic blocks mostly preserved their HP–LT assemblages. Candan *et al.* (1997) correlated the Selçuk Formation with a similarly metamorphosed olistostromal unit in Syros Island (Ridley & Dixon, 1984; Okrusch & Bröcker, 1990).

In the same region, on the Dilek peninsula (Fig. 2), this eclogite-bearing olistostrome tectonically overlies Mesozoic marble series ('Kayaaltı Formation'; Güngör & Erdoğan, 2001) intercalated with metapelites and

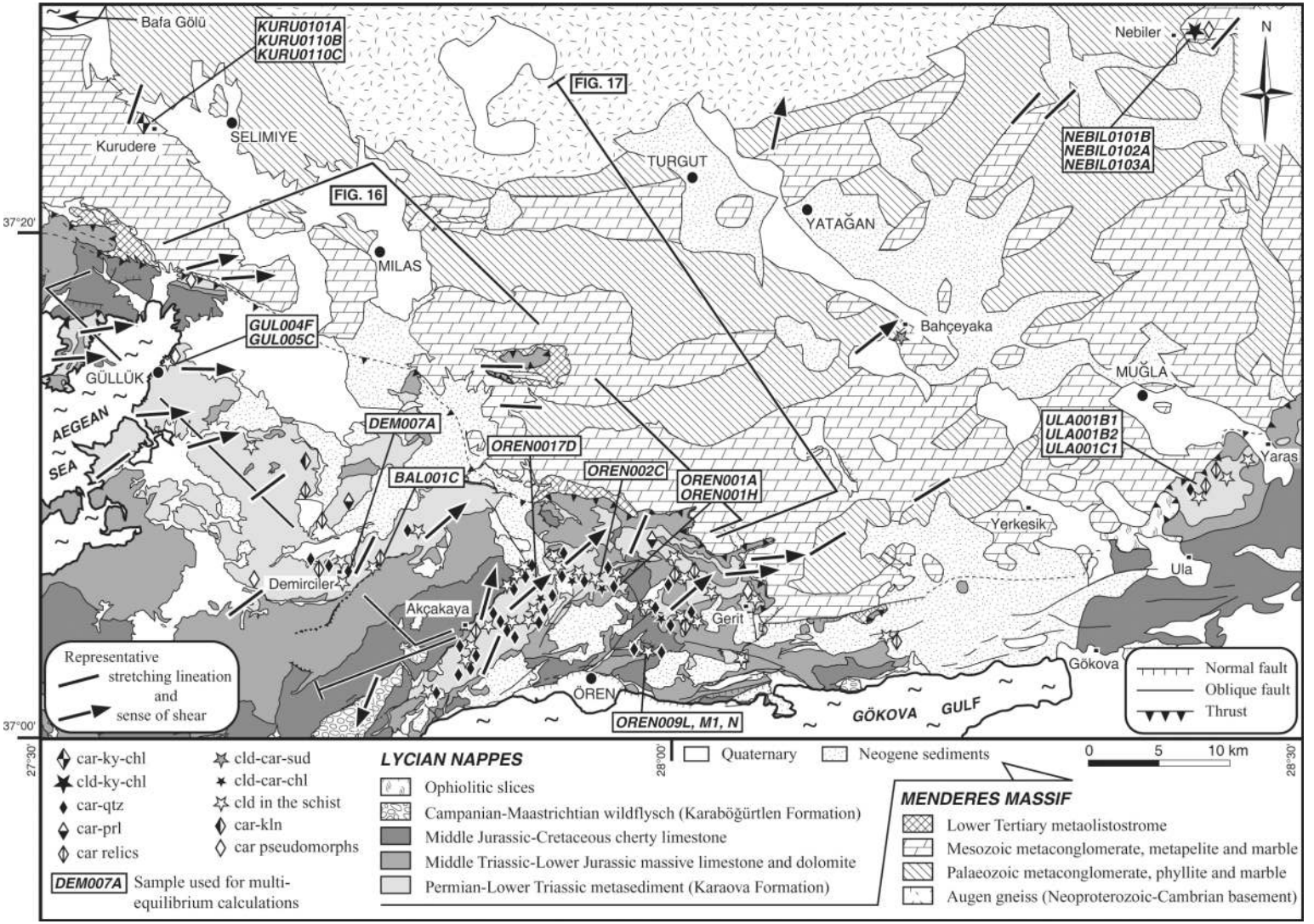

Fig. 4. Simplified tectono-metamorphic map showing the distribution of HP–LT assemblages and associated deformation in the Bodrum peninsula region [geology simplified after Çağlayan *et al.* (1980), Konak *et al.* (1987), Candan & Dora (1998) and N. Konak & N. Akdeniz (unpublished geological maps of MTA, Turkey); tectono-metamorphic data after Rimmelé *et al.* (2003*a*, 2003*b*)]. Locations of samples used for multi-equilibrium calculation are indicated on the map. car, Fe–Mg-carpholite; cld, chloritoid; chl, chlorite; sud, sudoite; kln, kaolinite; prl, pyrophyllite; ky, kyanite; qtz, quartz.

metabasites containing well-preserved blue amphiboles (Candan *et al.*, 1997; Oberhänsli *et al.*, 1998). This blueschist-facies metamorphism (10 kbar minimum/470°C; Candan *et al.*, 1997), dated as Middle Eocene (40 Ma, Ar/Ar on phengite; Oberhänsli *et al.*, 1998), was overprinted by a regional Barrovian-type metamorphism under greenschist-facies conditions during the Late Eocene–Early Oligocene (Candan *et al.*, 1997). A correlation with the blueschists of Samos Island (Mposkos & Perdikatsis, 1984; Okrusch *et al.*, 1984) belonging to the Cycladic complex has been proposed (Candan *et al.*, 1997; Oberhänsli *et al.*, 1998). Because of similar eclogite and blueschist metamorphic imprints described in the Aegean domain, many researchers have argued that the Dilek–Selçuk region forms the eastward lateral continuation of the Cycladic complex, and have excluded it from the geological definition of the Menderes Massif (Oberhänsli *et al.*, 1998; Ring *et al.*, 1999*a*, 1999*b*; Gessner *et al.*, 2001*a*; Okay, 2001), the Cycladic complex resting on top of the Menderes Massif (Fig. 2).

Before Alpine HP–LT metamorphism was described in the Upper Triassic metaconglomerate of the Menderes metasedimentary 'cover' (Rimmelé *et al.*, 2003*b*), the whole massif ('core' and the 'cover' rocks) was considered to have undergone only a Barrovian-type metamorphism [the so-called MMM, Main Menderes Metamorphism of Şengör *et al.* (1984)] with preserved upper amphibolite-facies conditions in the lower levels of the massif and greenschist-facies conditions in the uppermost parts of the cover series (Dürr, 1975; Akkök, 1983; Ashworth & Evirgen, 1984*a*; Şengör *et al.*, 1984; Satır & Friedrichsen, 1986; Konak *et al.*, 1987; Okay, 2001; Ring *et al.*, 2001; Whitney & Bozkurt, 2002; Régnier *et al.*, 2003).

In the southern submassif, the regional foliation is strongly deformed. Asymmetric kilometre-scale folds trend parallel to the Lycian nappe contact and are frequently overturned with a northward vergence (Bozkurt & Park, 1999; Whitney & Bozkurt, 2002; Rimmelé *et al.*, 2003*a*, 2003*b*). A pronounced stretching is associated with the regional foliation. In the HP–LT metaconglomerate, stretching lineations are roughly oriented N050° (Rimmelé *et al.*, 2003*b*). ENE–WSW stretching and senses of shear towards the ENE have also been reported in the uppermost levels of the marble envelope, just below the contact with the Lycian Nappes (Collins & Robertson, 2003; Rimmelé *et al.*, 2003*a*) (Fig. 4). The Palaeozoic schists and the augen gneisses of the Menderes Massif display a strong NNE–SSW to NE–SW stretching associated with top-to-the-north fabrics, these kinematic indicators being overprinted by top-to-the-south displacements. Some workers consider that the top-to-the-north movements were recorded during the Alpine orogeny (Bozkurt & Park, 1994, 1999; Bozkurt, 1996; Hetzel *et al.*, 1998; Lips *et al.*, 2001; Whitney & Bozkurt, 2002). In contrast, others claim that the top-to-the-north fabrics correspond to a pre-Alpine deformation and that the top-to-the-south senses of shear that crosscut the earlier fabrics in both 'core' and 'cover' units are related to the main Alpine contractional event (Ring *et al.*, 1999*a*; Gessner *et al.*, 2001*a*, 2001*b*, 2004).

The Lycian Nappes

At the south of the Menderes Massif, the Lycian Nappes tectonically overlie the metasediments of the Menderes cover (de Graciansky, 1972). Their origin has been the subject of many controversies. Whereas some workers argued that the tectonic slices originated from north of the Menderes Massif (de Graciansky, 1972; Dürr, 1975; Dürr *et al.*, 1978; Gutnic *et al.*, 1979; Şengör & Yılmaz, 1981; Okay, 1989; Collins & Robertson, 1997, 1998, 1999, 2003; Güngör & Erdoğan, 2001), others considered a dual origin (Poisson, 1977, 1985; Özkaya, 1990; Ersoy, 1993). A recent tectono-stratigraphic study by Collins & Robertson (1997, 1998, 1999, 2003) suggested that the Lycian Taurides represent an allochthonous Late Palaeozoic-Mesozoic rift–passive margin succession that was detached from its autochthon and translated towards the SE between Late Cretaceous and Late Miocene times. These workers defined the Lycian Allochthon as being made of three main units: (1) the 'Lycian Thrust Sheets' composed of Upper Palaeozoic to Tertiary sedimentary rocks; (2) a thick chaotic mélange unit (the 'Lycian Mélange') subdivided into a lower 'layered tectonic mélange' and an upper 'ophiolitic mélange'; tectonically overlain by (3) the 'Lycian Peridotite Thrust Sheet', which consists of serpentinized peridotites with a metamorphic sole. At the south of the Menderes Massif, the basal 'Lycian Thrust Sheets' widely crop out on the Bodrum peninsula (Figs. 2 and 4). They are composed of Upper Permian–Lower Triassic reddish to greenish metapelites [the Karaova Formation of Phillippson (1910–1915)] overlain by a thick succession of Middle Triassic–Middle Jurassic massive limestones and dolomites, grading upward to Upper Jurassic–Upper Cretaceous cherty limestones. The uppermost limestone layers are easily recognizable by calcite forming rosetta ('Rosetta limestones'). This thick limestone succession is overlain by the Campanian to Maastrichtian Karaböğürtlen wildflysch (de Graciansky, 1972; Bernoulli *et al.*, 1974; Çakmakoğlu, 1985; Okay, 1989). This sequence records a continuous sedimentation from Late Palaeozoic to Late Cretaceous (Fig. 3). Recent investigations in this area revealed the occurrence of a widespread HP–LT metamorphism documented by Fe–Mg-carpholite in the metasedimentary rocks of the basal Karaova Formation, which recorded pressures of about 8 kbar and maximum temperatures of 400°C (Oberhänsli *et al.*, 2001; Rimmelé

et al., 2003*a*). HP–LT relics have also been found in klippen of Lycian Nappes located above the Menderes Massif, and therefore extend over 200 km in both NS and EW directions (Fig. 1). An age between the Late Cretaceous and Eocene has been proposed for the HP–LT metamorphic event (Rimmelé *et al.*, 2003*a*). Prior to this discovery of high-pressure relics, the base of the Lycian Nappes was thought to have recorded only a weak low-grade metamorphism under greenschist-facies conditions (Ashworth & Evirgen, 1984*b*). In particular, Rimmelé *et al.* (2003*a*) reported the distribution of Fe–Mg-carpholite and its breakdown products throughout the Bodrum peninsula between Güllük and Muğla (Fig. 4), and noticed variations in the intensity of retrogression in the HP–LT metasediments suggesting different retrograde histories after a common HP–LT metamorphic peak. A high-pressure cooling path was suggested for the rocks showing well-preserved Fe–Mg-carpholite (Ören–Demirciler area) whereas a more isothermal decompression path was envisaged for the exhumation of rocks that show only Fe–Mg-carpholite pseudomorphs (e.g. Güllük area) (Rimmelé *et al.*, 2003*a*).

On the Bodrum peninsula, ductile deformation in the HP–LT metasediments of the Karaova Formation is associated with NE- to ENE-trending stretching with top-to-the-NE senses of shear, which are similar to the displacements observed in the southern Menderes Massif (Fig. 4). Most of this deformation is coeval with exhumation of the Karaova HP–LT rocks and appears to be localized along two major shear zones, one above the Karaova metapelites near Akçakaya ('Akçakaya shear zone'), and one along the contact with the Menderes Massif ('Gerit shear zone') (Rimmelé *et al.*, 2003*a*). It has been claimed that these top-to-the-NE to top-to-the-east movements are due to a northward backthrusting of the Lycian Nappes subsequent to their southward transport over the Menderes Massif, reactivating the Menderes Massif–Lycian Nappes contact as a top-to-the-NE shear zone that allowed exhumation of the Lycian metamorphic rocks (Rimmelé *et al.*, 2003*a*, 2003*b*). The earlier deformation associated with the southward translation of the nappe complex is preserved only in the uppermost levels (the Karaböğürtlen wildflysch) of the Lycian Thrust Sheets (Rimmelé *et al.*, 2003*a*; Fig. 4), and farther eastward in the Lycian mélange, as well as in peridotite slices (Collins & Robertson, 1998, 2003). This idea of a northward backthrusting of the Lycian Nappes has also been proposed by Bozkurt & Park (1999). On the Bodrum peninsula, Collins & Robertson (2003) also described some top-to-the-east senses of shear at the contact with the Menderes Massif but interpreted this deformation as part of the overall top-to-the-east to top-to-the-SE thrusting of the Lycian Nappes over the Menderes Massif.

REGIONAL DISTRIBUTION AND CHEMISTRY OF HP–LT ASSEMBLAGES

Samples were collected from about 300 outcrops throughout the region (Fig. 4) to describe the different parageneses involved in these HP–LT rocks. They were mainly collected in the HP–LT metamorphic Karaova Formation of the Lycian Nappes and in the HP–LT metaconglomerate of the Menderes Massif.

Distribution of HP–LT parageneses

Mineral distribution in the Lycian Nappes

Fe–Mg-carpholite and its retrogression products occur only at the base of the Lycian Nappes, within the metapelitic Karaova Formation. They are widespread on the Bodrum peninsula, between Güllük and Yaras (Fig. 4), and were locally found in a few klippen of Lycian Nappes that crop out at the top of the Menderes metamorphic rocks.

On the Bodrum peninsula, the distribution of HP–LT index minerals is not uniform (Fig. 4). Well-preserved Fe–Mg-carpholite was widely found between Ören and Demirciler, and commonly appears as centimetre- to decimetre-scale fibres in quartz segregations. It has also been observed within large crystals of calcite. However, in the lowermost parts of the pelitic sequence, close to the contact with the Menderes Massif, Fe–Mg-carpholite is partly to totally retrogressed to chlorite and pyrophyllite or to chlorite and phengite (e.g. near Güllük, Gerit or Ula). Chloritoid commonly occurs within the mineral foliation throughout the peninsula. It has also been found associated with Fe–Mg-carpholite in quartz segregations in the area of Ören.

In the northern part of the Menderes Massif, relics of Fe–Mg-carpholite were found in a small tectonic slice of Lycian sedimentary rocks NE of Borlu, and at Çivril (NE of Denizli), which represents the easternmost finding of Fe–Mg-carpholite in the region (Fig. 1).

In the Dilek peninsula region (Fig. 2), SW of Selçuk, two klippen of the Lycian Nappes occur on top of the Selçuk Formation. Outcrops of the Karaova Formation are exposed in both Lycian outliers. At the base of the northern klippe, near the village of Kirazlı (Fig. 5a), the strongly deformed chloritoid-bearing metapelites of the Karaova Formation preserved carpholite pseudomorphs at the contact with the rocks of the Menderes Massif. In contrast, in the southern slice (south of Tirhaköy; Fig. 5b), at an unknown distance from the Lycian–Menderes contact, fresh Fe–Mg-carpholite occurs in quartz segregations within the same reddish–greenish basal phyllites of the Karaova Formation.

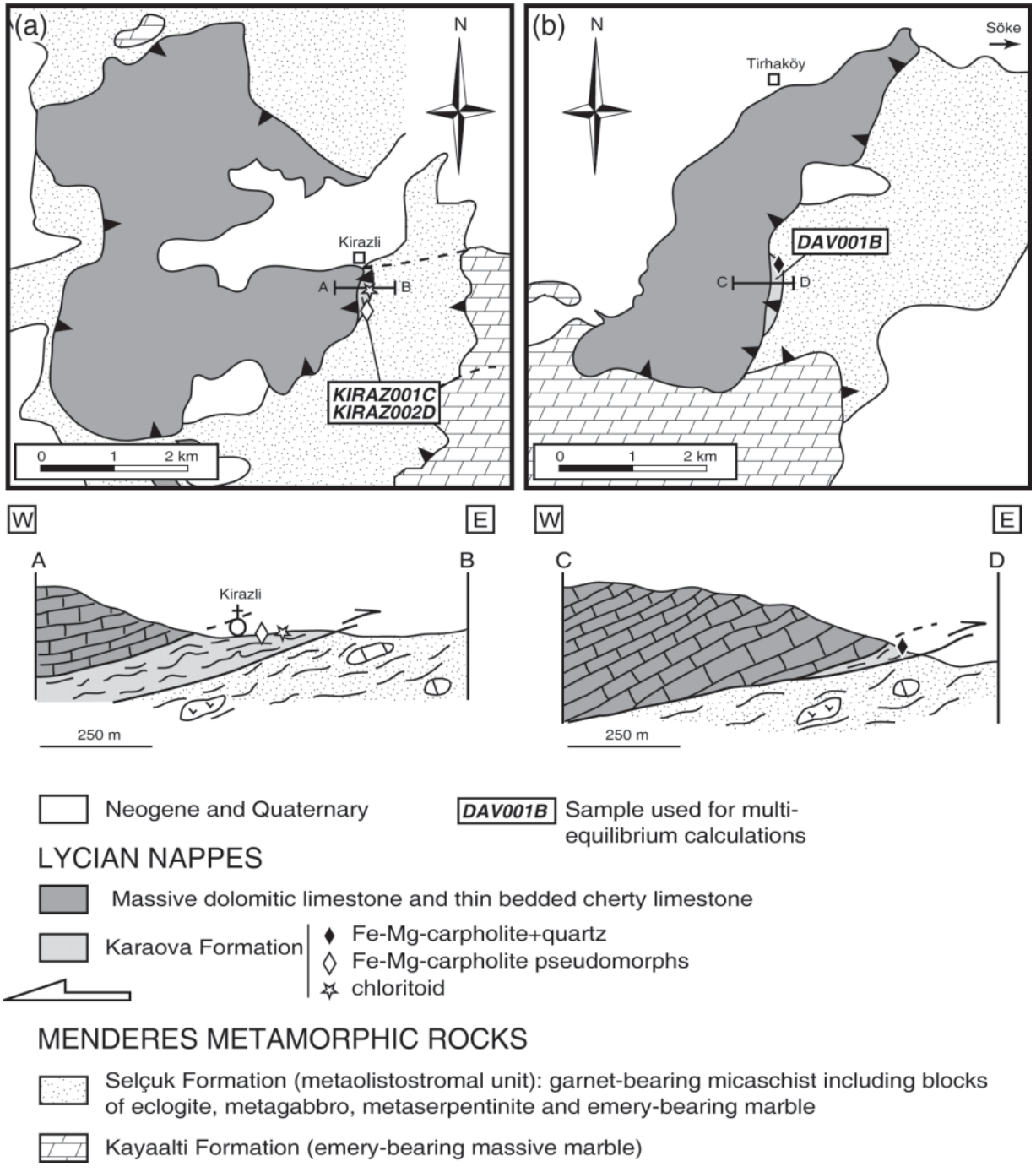

Fig. 5. Simplified geological maps of the two klippen of Lycian Nappes located in the Dilek–Selçuk area [modified after Güngör & Erdoğan (2001)]: (a) map of the northern klippe (Kirazlı area); (b) map of the southern klippe (Tirhaköy area). The localities of both klippen are indicated in Fig. 2. Locations of HP–LT relics and samples used for *P–T* estimates are shown on the maps as well as on the two schematic cross-sections across each HP–LT metamorphic unit.

Mineral distribution in the southern Menderes Massif

In the southern Menderes Massif, magnesiocarpholite occurrences have been found in three localities where the Upper Triassic metaconglomerate of the 'cover' series crops out just below a thick marble sequence (Rimmelé *et al.*, 2003*b*) (Fig. 4). South of Bafa Gölü, close to the village of Kurudere (Fig. 4), magnesiocarpholite–kyanite–chlorite–quartz assemblages were identified within

synfolial quartz veins. Magnesiocarpholite is partially preserved as relic hair-like microfibres within quartz in contact with kyanite. Elsewhere, it is commonly replaced by chlorite and kyanite. Chloritoid was not identified in this area. Farther east, SW of Bahçeyaka (Fig. 4), we found magnesiocarpholite–chloritoid–sudoite–quartz assemblages. Chloritoid results from the breakdown of magnesiocarpholite, which is preserved only within quartz. Finally, east of Nebiler (Fig. 4), we found chloritoid–kyanite–chlorite–quartz and kyanite–chlorite–quartz assemblages. In this area, prismatic aggregates of chlorite and kyanite occur as pseudomorphs of magnesiocarpholite. In the three areas, pyrophyllite and phengite are commonly associated with these HP–LT assemblages.

Mineral compositions in HP–LT rocks

Mineral analyses were obtained on three electron microprobes, a Cameca SX50 at Université Paris VI (Paris, France), a Cameca SX100 at the GeoForschungs-Zentrum (Potsdam, Germany), and a JEOL 8800 in the Humboldt Museum (Berlin, Germany). The three units operated under standard conditions (15 kV accelerating voltage, 10–20 nA specimen current, PAP correction procedure), using natural and synthetic standard minerals (in Paris: Fe_2O_3 [Fe], $MnTiO_3$ [Mn, Ti], diopside [Mg, Si], CaF_2 [F], orthoclase [Al, K], anorthite [Ca], albite [Na]; in Potsdam: Fe_2O_3 [Fe], rhodonite [Mn], rutile [Ti], MgO [Mg], wollastonite [Si, Ca], fluorite [F], orthoclase [Al, K], albite [Na]; in Berlin: anorthoclase [Si, Al, Na, K], ilmenite [Ti, Mn], magnetite [Fe], Cr-augite [Mg, Ca], apatite [F], tugtupite [Cl]). The analytical spot diameter was set between 3 and 5 μm keeping the same current conditions. About 50 samples were analysed and 23 of them were used for multi-equilibrium calculations. Only the latter are reported in Figs 4 and 5. The 50 samples are from the Karaova Formation of the Lycian Nappes and the metaconglomerate of the Menderes 'cover' sequence, which both contain HP–LT relics.

Fe–Mg-carpholite

The Fe–Mg-carpholite structural formula, $(Fe,Mn,Mg)Al_2Si_2O_6(OH,F)_4$, is calculated on the basis of five cations for the calculation of Si and three cations for Al, Fe, Mn and Mg, to account for the contribution of surrounding quartz when analysing fibres smaller than the microprobe beam diameter (Goffé & Oberhänsli, 1992). The Fe^{3+} ($Fe^{3+} = 2 - Al$) and Fe^{2+} contents are calculated after Goffé & Oberhänsli (1992). Analyses showing an oxide sum <85 wt % or >90 wt % were rejected. The compositions of Fe–Mg-carpholite from the Lycian Nappes and the Menderes Massif are reported in Fig. 6a. The complete dataset is included in Electronic Appendix 1, which can be downloaded from the *Journal of Petrology* website at http://www.petrology.oupjournals.org).

In the Lycian Nappes, Fe–Mg-carpholite composition is variable, as shown by X_{Mg} [$X_{Mg} = Mg/(Mg + Fe^{2+} + Mn)$] values ranging from 0·4 to 0·7. The X_{Mg} values vary from 0·65 to 0·7 in the klippe of the Lycian Nappes south of Tirhaköy, from 0·55 to 0·60 in the area of Demirciler, from 0·6 to 0·7 near the locality of Ula, from 0·6 to 0·65 in the Çivril area, and from 0·4 and 0·65 (mean value of 0·55) in the region of Ören (see Figs 1, 4 and 5b for locations). The Mn content in Fe–Mg-carpholite is very low ($0 < X_{Mn} < 0·03$) for all samples.

In the Menderes Massif, compositions of magnesiocarpholite are characterized by X_{Mg} values ranging from 0·65 to 0·90 (Rimmelé *et al.*, 2003*b*), and show a higher Mn content than in the Lycian Nappes (X_{Mn} reaching 0·25).

Chloritoid

The chloritoid formula, $(Fe,Mn,Mg)_2Al_4Si_2O_{10}(OH)_4$, is calculated on the basis of 12 oxygens. Fe^{3+}/Fe^{2+} ($Fe^{3+} = 4 - Al$) is calculated after Chopin *et al.* (1992). Analyses showing an oxide sum <90 wt % or >94 wt % were rejected (see chloritoid compositions in Electronic Appendix 2, available at http://www.petrology.oupjournals.org).

The samples from the Karaova Formation of the Lycian Nappes show X_{Mg} [$X_{Mg} = Mg/(Mg + Fe^{2+} + Mn)$] values roughly between 0·1 and 0·2 for the whole region. As for the Lycian Fe–Mg-carpholite, the X_{Mn} does not exceed 3% (Fig. 6b).

The chemical composition of chloritoid from the Menderes HP–LT rocks is rather different from the latter, showing higher values of X_{Mg} ($X_{Mg} \sim 0·45$) and X_{Mn} ($X_{Mn} \sim 0·25$) (Rimmelé *et al.*, 2003*b*).

Phyllosilicates

Structural formulae are calculated on the basis of 14 oxygens for chlorite and 11 for white mica. We only retained chlorite and white mica analyses with an oxide sum ranging between 83 and 89·5 wt % and between 92 and 97 wt %, respectively. To decrease the risk of using phengite and chlorite analyses with significant contaminations or alkali loss, we retained only the analyses that respect the chemical criteria reported by Vidal & Parra (2000). Chlorite analyses showing >0·5% ($Na_2O + K_2O + CaO$) and >0·1% K_2O were rejected, as well as white mica analyses showing >0·5% ($MnO + TiO_2 + Cl$). Finally, only the compositions of chlorites and phengites that could be expressed as linear combinations of the following end-members were retained: clinochlore $Mg_5Al_2Si_3O_{10}(OH)_8$, daphnite $Fe_5Al_2Si_3O_{10}(OH)_8$,

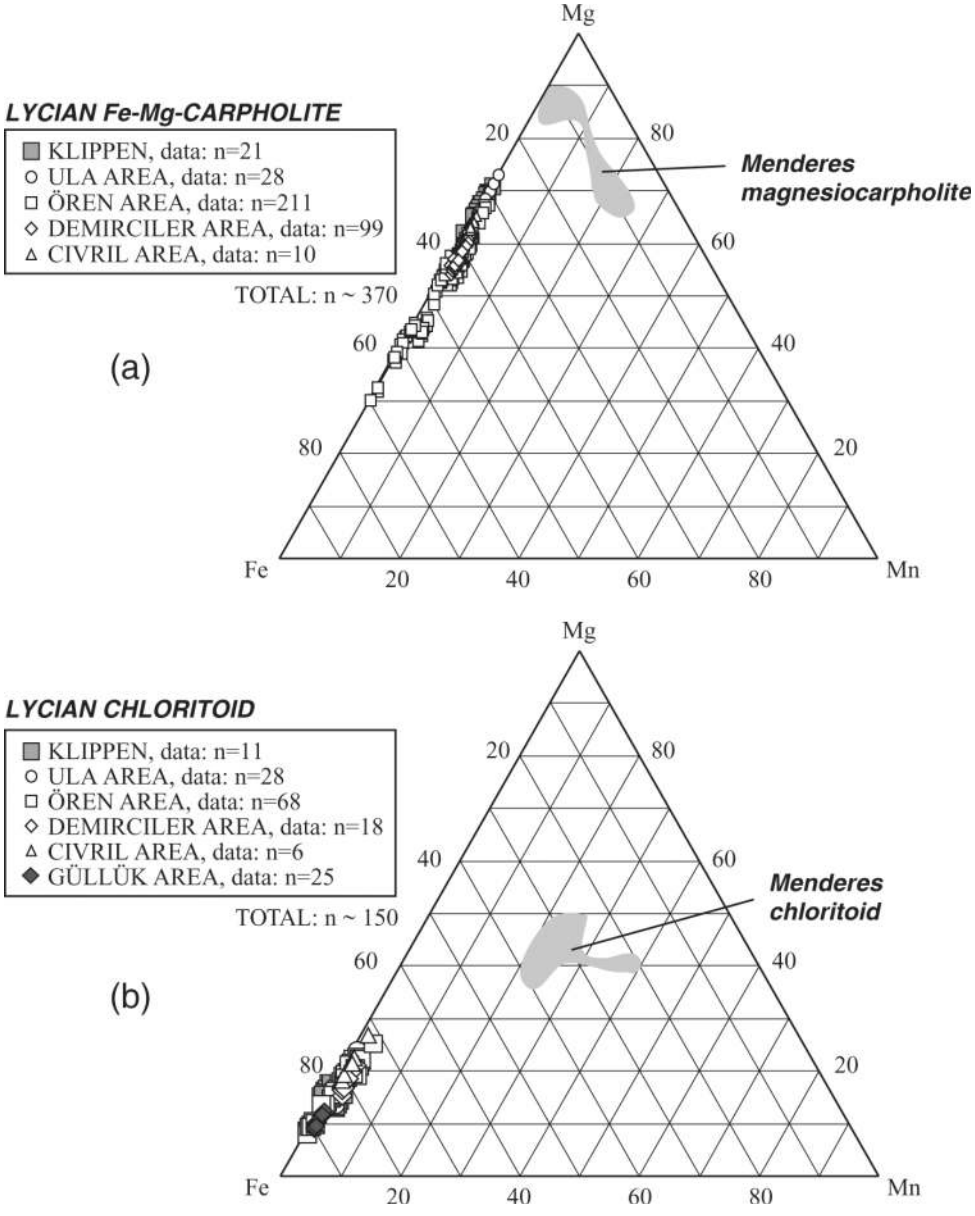

Fig. 6. Fe–Mn–Mg ternary diagrams showing compositions of Fe–Mg-carpholite (a) and chloritoid (b) from the Lycian Nappes (this study) and the Menderes Massif [after Rimmelé *et al.* (2003*b*)].

(Fe,Mg)-amesite $(Fe,Mg)_4Al_4Si_2O_{10}(OH)_8$, and sudoite $(Fe,Mg)_2Al_4Si_3O_{10}(OH)_8$ for chlorites; and (Fe,Mg)-celadonite $K(Fe,Mg)AlSi_4O_{10}(OH)_2$, muscovite $KAl_3Si_3O_{10}(OH)_2$, paragonite $NaAl_3Si_3O_{10}(OH)_2$, pyrophyllite $Al_2Si_4O_{10}(OH)_2$, and biotite $K(Fe,Mg)_3AlSi_3O_{10}(OH)_2$ for micas.

Tri-octahedral chlorite and sudoite compositions. Variations of chlorite compositions are mainly due to three major substitutions, the $FeMg_{-1}$ substitution (FM), the Tschermak substitution (TK) between clinochlore–daphnite and (Mg,Fe)-amesite $[Al^{IV}Al^{VI}Si_{-1}(Mg,Fe)_{-1}]$, and the di-trioctahedral substitution (DT) between clinochlore–daphnite and (Mg,Fe)-sudoite $[(Mg,Fe)_3V_{-1}Al_{-2}$, where V indicates a vacancy] (Vidal & Parra, 2000). The extent of substitutions depends on the metamorphic *P–T* conditions and on the bulk-rock chemistry (Vidal *et al.*, 2001). No data are available on the whole-rock chemistry of the Lycian HP–LT metasediments and the HP–LT metaconglomerate of the Menderes Massif. However, based on mineralogical observations (assemblages, modes, mineral chemistry), we infer that rocks from the Karaova Formation of the Lycian Nappes, as well as the HP–LT metaconglomerate of the Menderes 'cover' series, have a

roughly constant chemical composition throughout the study area.

In the whole area, about 500 chlorite and sudoite analyses have been made on samples from the Lycian Karaova Formation and about 120 on samples collected in the metaconglomerate of the Menderes Massif (Fig. 7; see also Electronic Appendix 3 at http://www.petrology.oupjournals.org). These analyses are plotted in (clinochlore–daphnite)–amesite–sudoite ternary diagrams and in Si vs X_{Mg} diagrams. The diagrams highlight the extent of the TK, DT and FM substitutions (Fig. 7a).

Chlorites from the Lycian Nappes have a composition lying between the amesite and the clinochlore–daphnite end-members (Fig. 7b). The sudoite content roughly ranges between 10 and 30 mol %, except for some analyses that reach 60 mol %. It is noteworthy that the sudoite content is high compared with natural chlorite compositions (sudoite content <35 mol %) described by Vidal *et al.* (2001). The question arises here whether these chlorite analyses result from contamination or interstratification. For this reason, we preferred not to use them for *P–T* estimates. Further studies would be necessary to characterize precisely this 'chlorite' that could exhibit either a tri- or di/tri-octahedral structure. Figure 7c shows X_{Mg} values [$X_{Mg} = Mg/(Mg + Fe^{2+} + Mn)$] ranging between 0·35 and 0·75 and Si contents between 2·5 and 3 a.p.f.u. The chlorite analyses from the Güllük region are Fe richer than those from other areas ($0{\cdot}35 < X_{Mg} < 0{\cdot}45$).

Sudoite compositions have a Si content ranging between 3 and 3·2 a.p.f.u. and X_{Mg} values between 0·6 and 0·85 (Fig. 7d). As mentioned by Vidal *et al.* (2001), the chlorite solid solution model cannot be used when the Si content of sudoite is >3·0 a.p.f.u. Therefore the sudoite analyses from the Lycian Nappes were not used for *P–T* estimates.

In the HP–LT rocks from the Menderes Massif, chlorite compositions exhibit smaller variations of TK, DT and FM substitutions than those from the Lycian Nappes, although the dataset of chlorite analyses in samples from the Menderes Massif is smaller than that of the Lycian Nappes. Compositions have a lower sudoite content than those from the Lycian Nappes (Fig. 7e). The Si content ranges between 2·6 and 2·8 a.p.f.u. and the X_{Mg} values cluster between 0·8 and 0·9 (Fig. 7f).

The very few sudoite analyses show a Si content around 3·1 a.p.f.u. The X_{Mg} is about 0·9 (Fig. 7g). For the same reasons as given above, sudoite compositions from the Menderes Massif were not used for *P–T* calculations.

White mica and pyrophyllite compositions. Variations of K-white mica (phengite) compositions are essentially a function of the $FeMg_{-1}$ substitution (FM), the Tschermak substitution (TK) between muscovite and (Mg,Fe)-celadonite [$Al^{IV}Al^{VI}Si_{-1}(Mg,Fe)_{-1}$], the pyrophyllitic substitution (P) between muscovite and pyrophyllite ($KAlSi_{-1}V_{-1}$), and the paragonitic substitution (Pa) between muscovite and paragonite (NaK_{-1}) (Vidal & Parra, 2000). The extent of substitutions in micas also depends on the *P–T* conditions as well as on the rock chemistry (Parra *et al.*, 2002*a*).

Two white micas have been recognized in the Menderes Massif and the Lycian Nappes: phengite and paragonite. Very low quantities of paragonite have been detected by X-ray diffraction (XRD) analyses in only a few samples. Pyrophyllite also occurs in the samples collected in both the Lycian Nappes and the Menderes Massif.

About 650 analyses of white mica and pyrophyllite have been performed in the Lycian samples and about 75 in samples from the Menderes Massif (analyses in Electronic Appendix 4 at http://www.petrology.oupjournals.org). These analyses are plotted in pyrophyllite–celadonite–muscovite and pyrophyllite–paragonite–muscovite ternary diagrams showing the extent of the TK, P and Pa substitutions (Fig. 8a).

For the Karaova Formation of the Lycian Nappes, Fig. 8b shows that the pyrophyllite content in phengite can reach high values (~40 mol %) whereas the celadonite content is not higher than 10 mol %. The paragonitic content in phengite is always low (mainly <20 mol %) (Fig. 8c).

In the Menderes metaconglomerate, phengites have generally a lower pyrophyllite content than in the Lycian Nappes (0–30 mol %) whereas the celadonite and muscovite contents are higher (Fig. 8d). As for the Lycian Nappes, phengites have a low paragonite content (10–20 mol %) (Fig. 8e).

In both the Lycian Nappes and the Menderes Massif, the pyrophyllite compositions have very low K and Na contents (<10 mol %; Fig. 8c and e).

Interpretation in terms of *P–T* evolution

The Fe–Mg-carpholite and chloritoid compositions in the Menderes Massif show higher X_{Mg} values than in the Lycian Nappes (Fig. 6), which document higher *P–T* conditions in the Menderes Massif than in the Lycian Nappes (Chopin *et al.*, 1992; Theye *et al.*, 1992; Vidal *et al.*, 1992, 1994; Oberhänsli *et al.*, 1995). Furthermore, in the Lycian Nappes, Fe–Mg-carpholite is mainly associated with pyrophyllite whereas it forms assemblages with kyanite in the Menderes Massif, which also suggests higher temperature conditions. The sudoite content in chlorite from the Lycian Nappes is higher than in that from the Menderes Massif (Fig. 7), which also documents lower temperature conditions for the Lycian HP–LT metamorphism (Vidal *et al.*, 2001). The higher pyrophyllite content and lower muscovite content in phengites of the Lycian Nappes than in those from the Menderes Massif

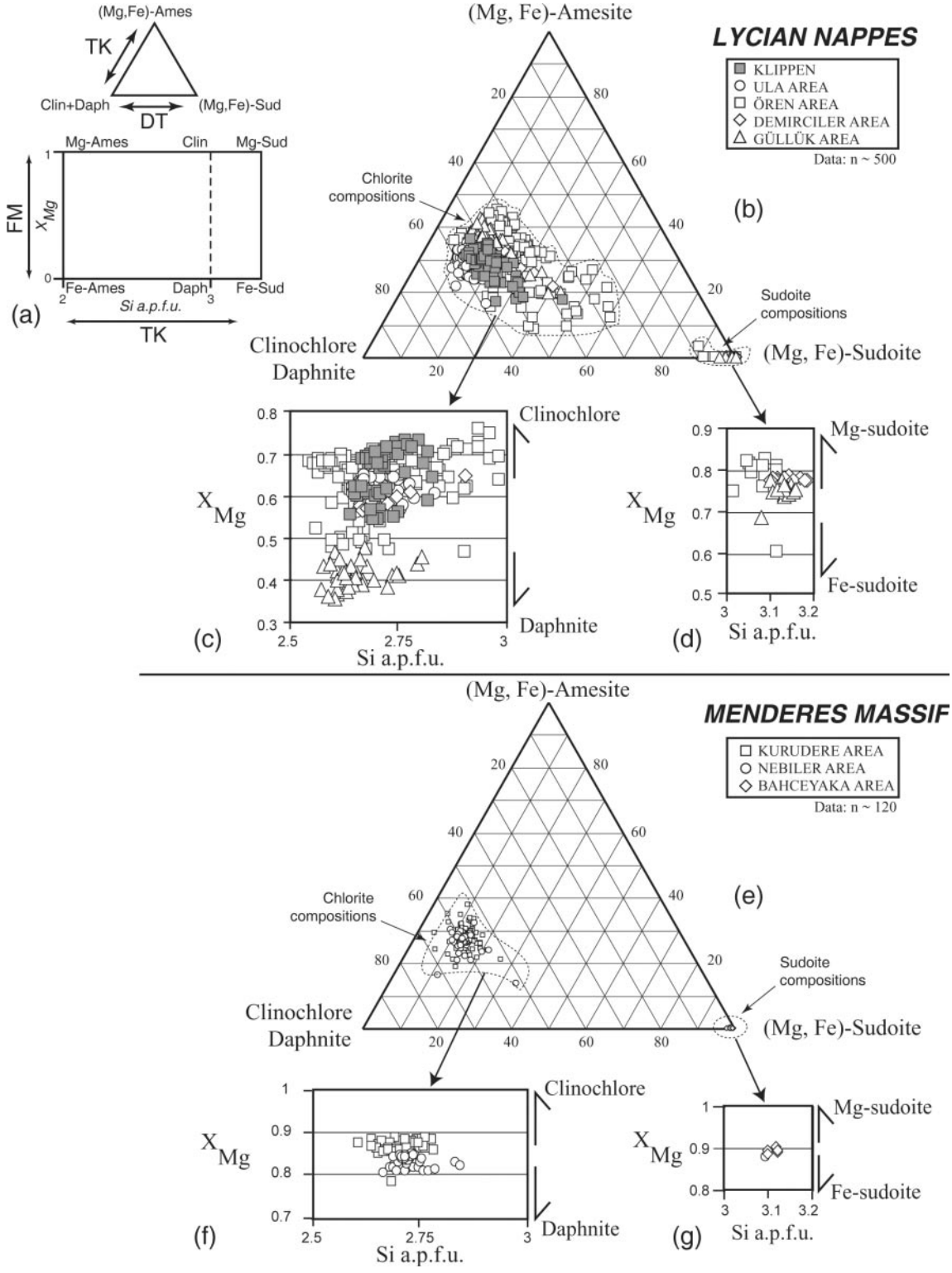

Fig. 7. (a) Diagrams showing the three systematic main substitutions between the chlorite end-members (TK, Tschermak substitution; DT, di-trioctahedral substitution; FM, $FeMg_{-1}$ substitution). (b) Chemical variability of chlorite and sudoite from the Lycian Nappes caused by the TK and DT substitutions. Compositional variability of chlorite (c) and sudoite (d) from the Lycian Nappes caused by the TK and FM substitutions. (e) Compositional variability of chlorite and sudoite from the Menderes Massif caused by the TK and DT substitutions. Compositional variability of chlorite (f) and sudoite (g) from the Menderes Massif caused by the TK and FM substitutions.

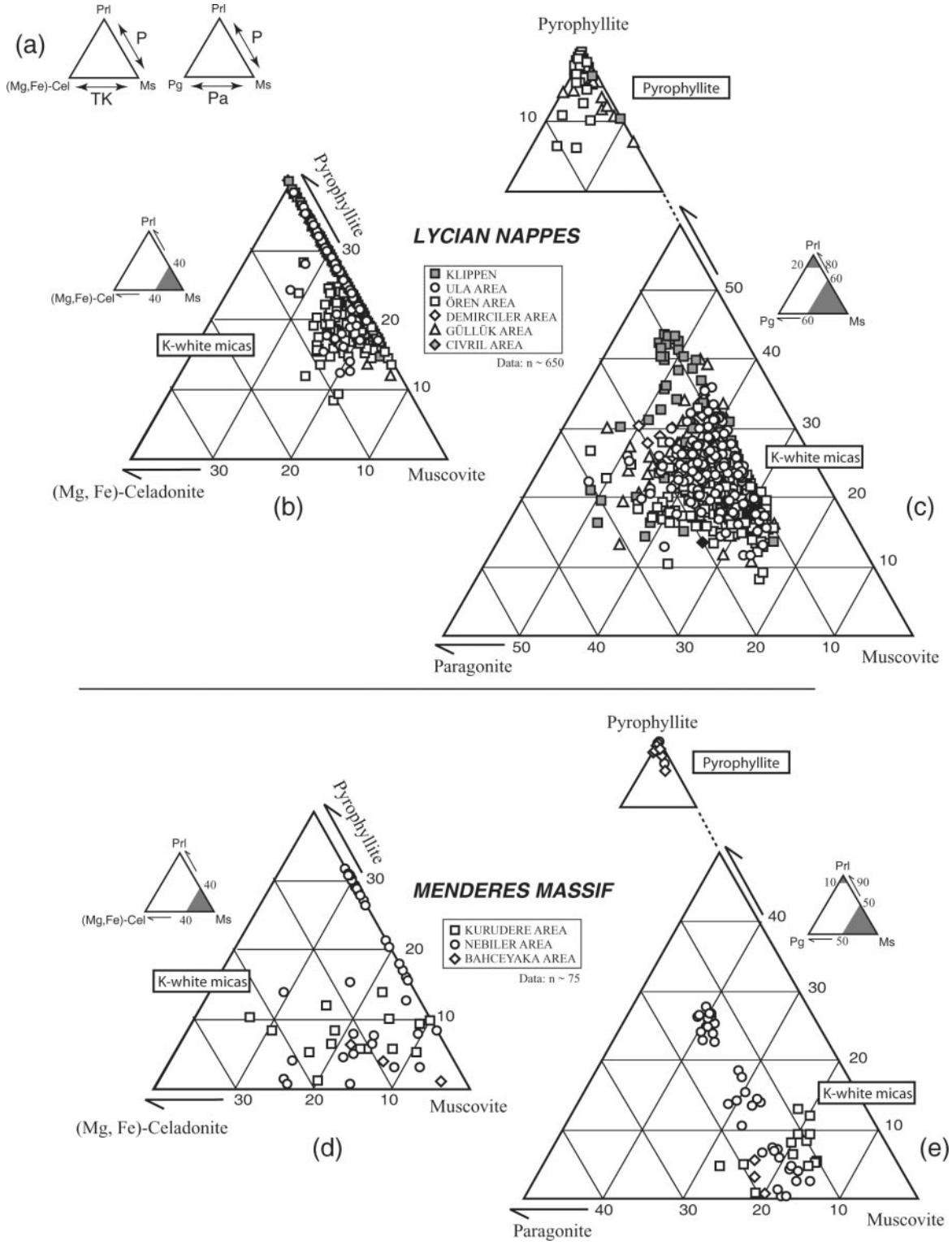

Fig. 8. (a) Ternary diagrams showing the systematic Tschermak (TK), pyrophyllitic (P) and paragonitic (Pa) substitutions in K- and Na-white micas [Prl, pyrophyllite; Ms, muscovite; (Mg–Fe)-Cel, celadonite; Pg, paragonite]. Compositional variability of K-white micas (phengite) from the Lycian Nappes caused by the TK and P substitutions (b) and by the P and Pa substitutions (c). Pyrophyllite compositions from the Lycian Nappes are also reported in (c). Compositional variability of K-white micas from the Menderes Massif caused by the TK and P substitutions (d) and by the P and Pa substitutions (e). Pyrophyllite compositions from the Menderes Massif are also plotted in (e).

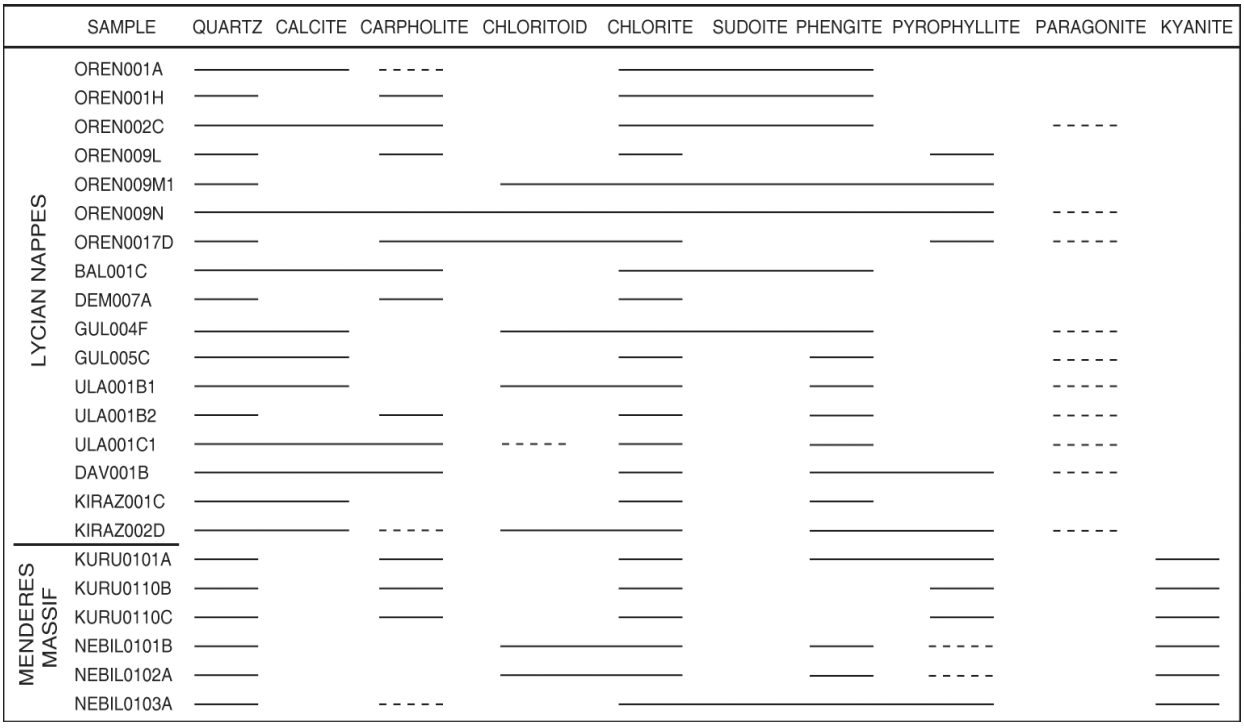

Fig. 9. Mineral occurrences in samples used for multi-equilibrium calculations. Dashed lines represent mineral in low abundance.

(Fig. 8) also suggests lower P–T conditions for the Lycian Nappes (Vidal & Parra, 2000; Parra *et al.*, 2002*a*). Furthermore, the TK substitution between muscovite and celadonite has a slightly wider extent in the Menderes metaconglomerate than in the Lycian metasediments (Fig. 8b and d), thus indicating higher pressure conditions for the Menderes HP–LT rocks than for the Lycian metamorphic rocks (Massonne & Szpurka, 1997; Vidal & Parra, 2000; Parra *et al.*, 2002*a*).

These differences in the mineral compositions from the Lycian Nappes and the Menderes Massif clearly point to different metamorphic conditions in the two tectonic units. However, a combination of these variations in mineral composition at the local equilibria scale provides a better-constrained picture of the P–T conditions reached during HP–LT metamorphism and its exhumation.

P–T ESTIMATES BASED ON MULTI-EQUILIBRIUM CALCULATIONS

Sampling

In the study area, 23 samples collected in the HP–LT metamorphic Karaova Formation of the Lycian Nappes and in the HP–LT metaconglomerate of the Menderes Massif were used to constrain P–T estimates based on multi-equilibrium calculations. The locations of these samples are shown in Figs 4 and 5. All samples have been analysed by XRD (Siemens, D5005 model, University of Potsdam). The mineral occurrences for each thin section are listed in Fig. 9.

Thermodynamic data and solid-solution properties

The thermodynamic dataset and solid-solution properties used in this work are from the TWEEQ (Thermobarometry With Estimation of EQuilibration state; Berman, 1991) updated database of Berman (1988). For the following minerals, external data were included: chlorite (Vidal *et al.*, 2001), sudoite (Vidal *et al.*, 1992), phengite (Parra *et al.*, 2002*a*), Fe–Mg-carpholite (Vidal *et al.*, 1992), and chloritoid (Mg-chloritoid from Vidal *et al.*, 2001; Fe-chloritoid from Vidal *et al.*, 1994). Activities of Fe–Mg-carpholite were calculated after Vidal *et al.* (1992) [$a_{(car)} = (X_{Mg})(X_{Al})^2(X_{OH})^4$ with $X_{Mg} = Mg/(Mg + Fe^{2+} + Mn)$, $X_{Al} = (2 - Fe^{3+})/2$ and $X_{OH} = (4 - F)/4$]. The X_{Mg} and X_{Fe} of chloritoid were calculated considering the Mn content [$X_{Mg} = Mg/(Mg + Fe^{2+} + Mn)$ and $X_{Fe} = Fe/(Mg + Fe^{2+} + Mn)$], and activities are from Vidal *et al.* (1994) ($a_{[Mg\text{-}Cld]} = X_{Mg}$ and $a_{[Fe\text{-}Cld]} = X_{Fe}$). As thermodynamic data for Fe-amesite are unpublished and still provisory (O. Vidal & T. Parra, personal

communication), we did not take into account this end-member for our calculations.

Method of calculation

The calculation procedure is a systematic method that allows simultaneous estimates of P and T using a small number of phases that are systematically present in the studied thin sections, and to check for equilibrium. It is based on the notion of 'multi-equilibrium calculations' (Berman, 1991), which requires the assumption of local equilibrium and the use of solid-solution models and thermodynamic data for minerals characterized by compositional variations. The method involves the plotting of all the equilibrium reactions (TER, total equilibrium reactions) calculated with the end-members used to describe the composition of chlorite and phengite (often associated with other minerals). Increasing the number of end-members used to express the compositional variability of chlorite, phengite and other associated minerals allows one to increase the number of TER that can be computed for a given paragenesis involving these minerals, and therefore the number of linearly independent equilibrium reactions (IER) (Vidal & Parra, 2000; Vidal *et al.*, 2001; Parra *et al.*, 2002*a*, 2002*b*) (Fig. 10).

The pairs or triplets used to perform the calculations were first selected using classical microtextural criteria suggesting equilibrium state. In particular, the assemblage-forming minerals must be in contact and be involved in the same microstructure as shown in Fig. 10.

Assuming that the standard state thermodynamic data as well as the activity–composition relationships are well calibrated, all the reactions computed for a given paragenesis should intersect at a single point in the P–T field if equilibrium is achieved (Fig. 10). However, cumulated errors on each equilibrium reaction involve scatters in the intersection points. The InterSX (Berman, 1991) program included in the TWEEQ package allows one to calculate P, T and the scatters, scat(P) and scat(T), between intersections.

Even if the thermodynamic database was perfect, imprecision in the mineral analyses limits the relative precision of the P–T estimates. The precision of the microprobe analysis induces scatter related to variations of mica, chlorite and other mineral compositions, which can be calculated using a Monte Carlo simulation (Lieberman & Petrakakis, 1991; Vidal & Parra, 2000; Parra *et al.*, 2002*b*). This calculation was made for each paragenesis used for P–T estimates and led to a determination of paragenesis-dependent maximum permissible scatters, above which the minerals are considered to be out of equilibrium (Vidal & Parra, 2000).

For each paragenesis, we first chose the assemblages showing mineral compositions that were 'perfectly' equilibrated (i.e. all equilibria intersect at a single point). As an example, for a paragenesis Fe–Mg-carpholite–phengite–chlorite, we took the three compositions that showed the best equilibrium between each mineral. A Gaussian error distribution with $1\sigma = 1\%$ relative for all major oxides was randomly sampled about the nominal weight percentage for each oxide in phengite, chlorite and Fe–Mg-carpholite (except for volatile Na_2O and K_2O in phengite, for which $1\sigma = 2\%$ relative). Minor elements were not considered because even large relative variations have a negligible influence on the Monte Carlo simulation. A hundred permutations allowed simulation of 100 mineral compositions. The set of 100 simulated chlorite–phengite–carpholite triplets was used to calculate 100 separate P–T points, as well as their associated scatters in P and T [scat(P) and scat(T)] with the InterSX program. These best P–T estimates (Pi and Ti, $i = 1$–100) are defined as a solid weighted average. Because the distribution of these best estimates can be approximated by a Gaussian distribution (Lieberman & Petrakakis, 1991), we calculated a mean pressure $\overline{P} = [\Sigma Pi]/100$ and a mean temperature $\overline{T} = [\Sigma Ti]/100$ for the 100 Pi and Ti, as well as the 95% confidence standard deviations (σP and σT) and the correlation coefficient $\rho(P,T)$. These values are used to estimate a P–T ellipse depicting the precision of any P and T calculation for the given paragenesis. The size is calculated with σP and σT. The orientation of the ellipse is constrained by the correlation coefficient $\rho(P,T)$ (Powell & Holland, 1988, 1994). We also calculated the average scatters $\bar{s}\text{cat}(P) = [\Sigma\text{scat}(Pi)]/100$ and $\bar{s}\text{cat}(T) = [\Sigma\text{scat}(Ti)]/100$, and their standard deviations $\sigma_{\text{scat}(P)}$ and $\sigma_{\text{scat}(T)}$, to determine the maximum permissible scatter [$\text{scat}(P)_{\max} = \bar{s}\text{cat}(P) + 2\sigma_{\text{scat}(P)}$ and $\text{scat}(T)_{\max} = \bar{s}\text{cat}(T) + 2\sigma_{\text{scat}(T)}$] of any P–T estimate with a 95% confidence level (2σ).

For any other P–T estimate from the same paragenesis, we then compared the scatters scat(P) and scat(T) with the maxima defined previously. If $\text{scat}(P) > \text{scat}(P)_{\max}$ or $\text{scat}(T) > \text{scat}(T)_{\max}$, the minerals involved in the paragenesis were considered to be out of equilibrium and the calculated P–T conditions were rejected.

In the study area, P–T conditions were estimated from six different parageneses: Fe–Mg-carpholite–chlorite–phengite–quartz, magnesiocarpholite–chlorite–kyanite–quartz, Fe–Mg-carpholite–chlorite–quartz, chlorite–phengite–quartz, chloritoid–chlorite–phengite–quartz, and chloritoid–chlorite–quartz. For each paragenesis, the Monte Carlo simulation was performed to estimate the analytical uncertainties and the paragenesis-dependent maximum permissible scatters (different from one paragenesis to the other) (Table 1). The amount of rejected P–T estimates is large and may result from calculations performed with non-equilibrated minerals. However, as already described by Parra *et al.* (2002*b*), a significant proportion of rejected mineral pairs or triplets showing $\text{scat}(P) > \text{scat}(P)_{\max}$ or $\text{scat}(T) > \text{scat}(T)_{\max}$

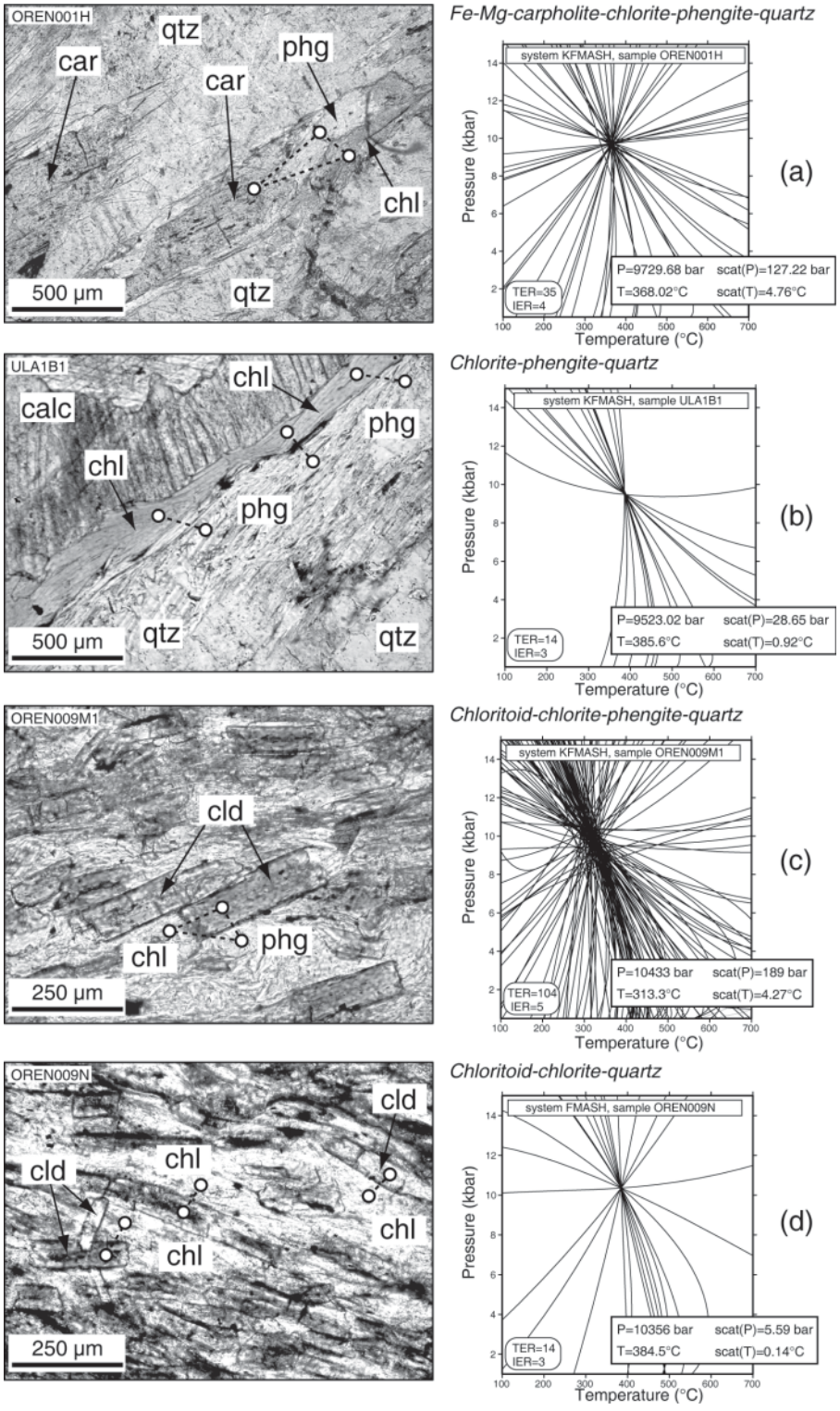

Fig. 10. Photomicrographs showing the location of mineral analyses (left) and *P–T* diagrams showing the plot of all equilibrium reactions computed (right) for a paragenesis of Fe–Mg-carpholite–chlorite–phengite–quartz (a), chlorite–phengite–quartz (b), chloritoid–chlorite–phengite–quartz (c) and chloritoid–chlorite–quartz (d). *P–T* estimates and the scatters between intersections [scat(*P*) and scat(*T*)] reported on each *P–T* diagram are calculated with the InterSX (Berman, 1991) program included in the TWEEQ package. For these examples, calculations were made in the KFMASH (K_2O–FeO–MgO–Al_2O_3–SiO_2–H_2O) system (a–c) and in the FMASH (FeO–MgO–Al_2O_3–SiO_2–H_2O) system (d). car, Fe–Mg-carpholite; phg, phengite; cld, chloritoid; chl, chlorite, qtz, quartz; calc, calcite; TER, number of total equilibrium reactions; IER, number of independent equilibrium reactions.

Table 1: Results of the Monte Carlo simulation accounting for analytical uncertainties for each paragenesis used in the P–T *calculations (see text for explanation)*

Paragenesis	$\overline{P}$ (bar)	$\overline{T}$ (°C)	$\overline{\text{scat}}$ (P) (bar)	$\overline{\text{scat}}$ (T) (°C)	σP (bar)	σT (°C)	$\sigma_{\text{scat}(P)}$ (bar)	$\sigma_{\text{scat}(T)}$ (°C)	$\rho(P,T)$	scat(P)$_{\max}$ (bar)	scat(T)$_{\max}$ (°C)
Fe–Mg-carpholite–chlorite–phengite–quartz	9961	369·8	213·9	8·1	346·5	7·9	78·3	3·1	0·87	370·4	14·2
Mg-carpholite–chlorite–kyanite–quartz	13767·2	485·9	224·2	7·9	648·2	7·2	133·7	4·4	0·99	491·7	16·7
Fe–Mg-carpholite–chlorite–quartz	10108·5	325·2	3·3	0·1	278·1	14·8	1·9	0·05	0·98	—	—
Chlorite–phengite–quartz	8756·8	405·7	177·4	5·6	640·5	26·9	88	2·9	–0·76	353·3	11·3
Chloritoid–chlorite–phengite–quartz	10472·3	315·7	505·6	9·5	57	5·9	225·9	4·5	–0·13	957·4	18·5
Chloritoid–chlorite–quartz	10592	390·6	313·5	14	264·5	9·7	179·3	10·4	0·84	672·2	34·9

revealed P–T conditions within the P–T trend defined by the equilibria that showed scat(P) < scat(P)$_{\max}$ or scat(T) < scat(T)$_{\max}$. This is probably due to an underestimation of the maximum scatter [i.e. scat(P)$_{\max}$ and scat(T)$_{\max}$ being too low] that causes rejection of pairs and triplets of minerals that are actually in equilibrium.

P–T estimates

After the selection of all P–T estimates by the Monte Carlo method, those considered to be in equilibrium are reported on a P–T field. We present in the following various P–T paths resulting from multi-equilibrium calculations performed from samples collected in different regions (see Figs 4 and 5 for location of samples). For each sample, the calculated P–T conditions and their paragenesis-dependent error bars ($\pm 1\sigma$) resulting from the Monte Carlo simulation are plotted on a P–T diagram. The 95% confidence ellipses and the number of independent equilibrium reactions for each calculation are reported in the P–T diagram. It is noteworthy that achievement of equilibrium is not certified for P–T results calculated with only two independent equilibrium reactions. However, most of the P–T calculations with two independent equilibrium reactions show P–T points located within the trend defined by those calculated with more than two independent equilibrium reactions.

P–T *results in the Lycian Nappes*

The region of Ören–Demirciler. In the region located between Ören and Demirciler (Fig. 4), the trends defined by the P–T estimates from different mineral pairs or triplets are reported in Fig. 11. Each P–T diagram corresponds to P–T calculations made for samples from the same outcrop. Depending on the parageneses, calculations were made either with Fe–Mg-carpholite–chlorite–phengite and chloritoid–chlorite–phengite triplets, or with Fe–Mg-carpholite–chlorite, chlorite–phengite and chloritoid–chlorite pairs. Chlorite and phengite are commonly derived from the retrogression of Fe–Mg-carpholite (see photomicrograph of Fig. 10a). These three minerals form common triplets in the thin sections. Chloritoid–chlorite pairs are observed in the foliation. Chloritoid–chlorite–phengite triplets could rarely be used in the P–T calculations because of contaminated analyses of phengite owing to its very small size within the foliation.

North of Ören, in the Karaova metasediments where well-preserved Fe–Mg-carpholite occurs, P–T conditions estimated from different thin sections are shown in Fig. 11a–d. The best-constrained P–T estimates (with IER > 2) are located in a domain from 12 kbar/420°C to 8–9 kbar/300°C. Other P–T points calculated with only two independent reactions are located in this P–T trend and show a wider range of P–T conditions from

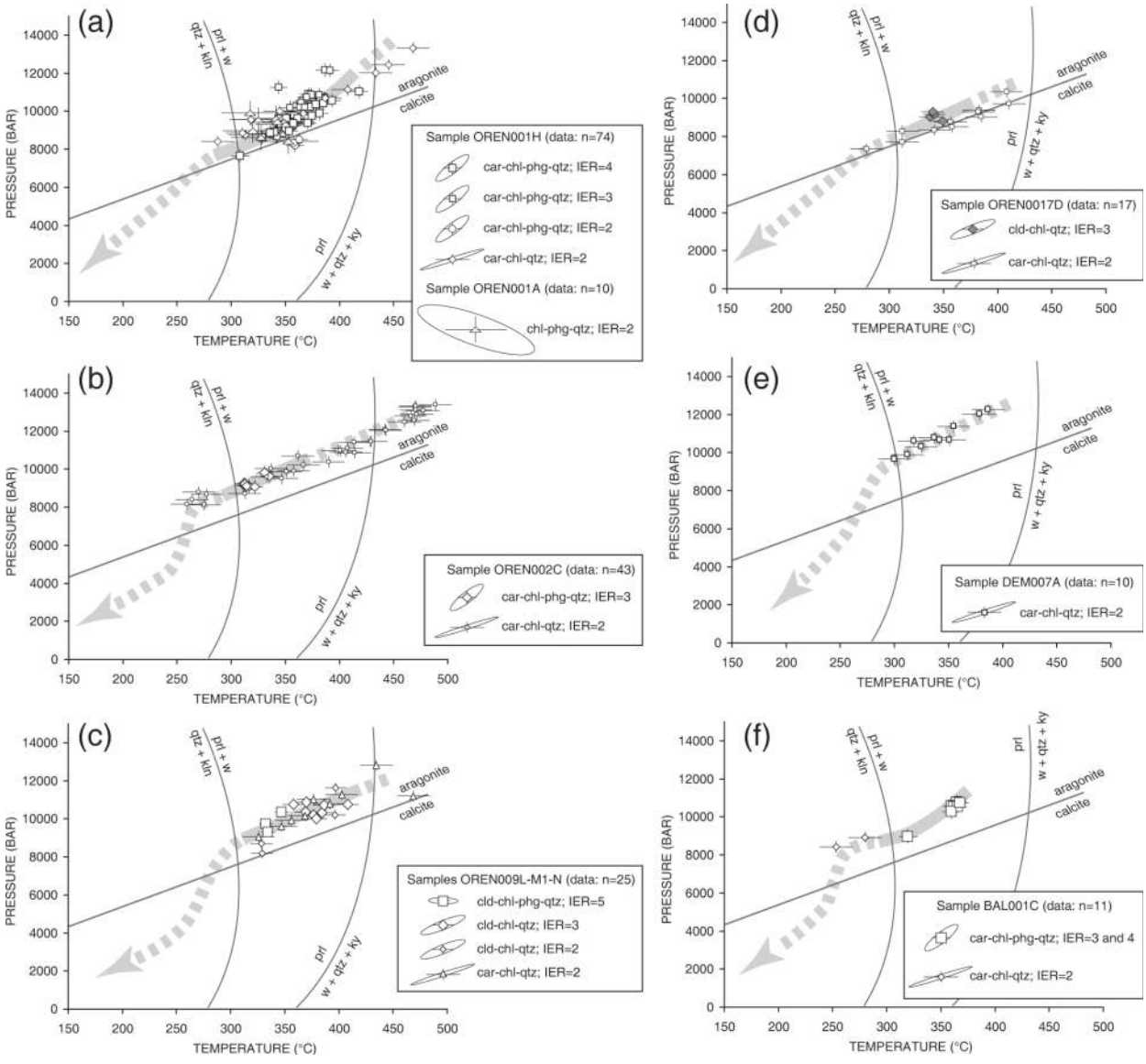

Fig. 11. *P–T* estimates for samples from the Ören area (a–d) and the Demirciler area (e, f) [Lycian Nappes]. The paragenesis-dependent error bars (±1σ) and 95% confidence ellipses are calculated with the Monte Carlo simulation. The number of independent equilibrium reactions (IER) for each calculation is reported in the legend.

13–14 kbar/470°C to 8 kbar/250°C, which are not significantly different from the better constrained data considering the 95% confidence ellipses.

In the Demirciler area, the two samples DEM007A and BAL001C revealed the same range of metamorphic conditions for the same parageneses (Fig. 11e and f). Altogether, the *P–T* conditions estimated in the well-preserved Fe–Mg-carpholite-bearing metasediments of the Ören–Demirciler region indicate a metamorphic peak of about 12–13 kbar/400–420°C followed by a progressive decrease of temperature still at HP–LT conditions. The fact that the *P–T* paths correspond to exhumation paths is supported by the commonly observed retrogression of HP–LT minerals to chlorite and phengite (Fig. 10a as an example). As shown in Fig. 11, the cooling exhumation paths are located in the aragonite stability field. During our investigations in this area of the Lycian Nappes, we found widespread occurrences of decimetre- to metre-scale crystals of calcite forming rosetta in Cretaceous cherty limestones that are part of the thick carbonate sequence that overlies the Karaova Formation (Fig. 3). A few samples containing these long crystals forming radial structures have been analysed using XRD and Raman spectrometry methods

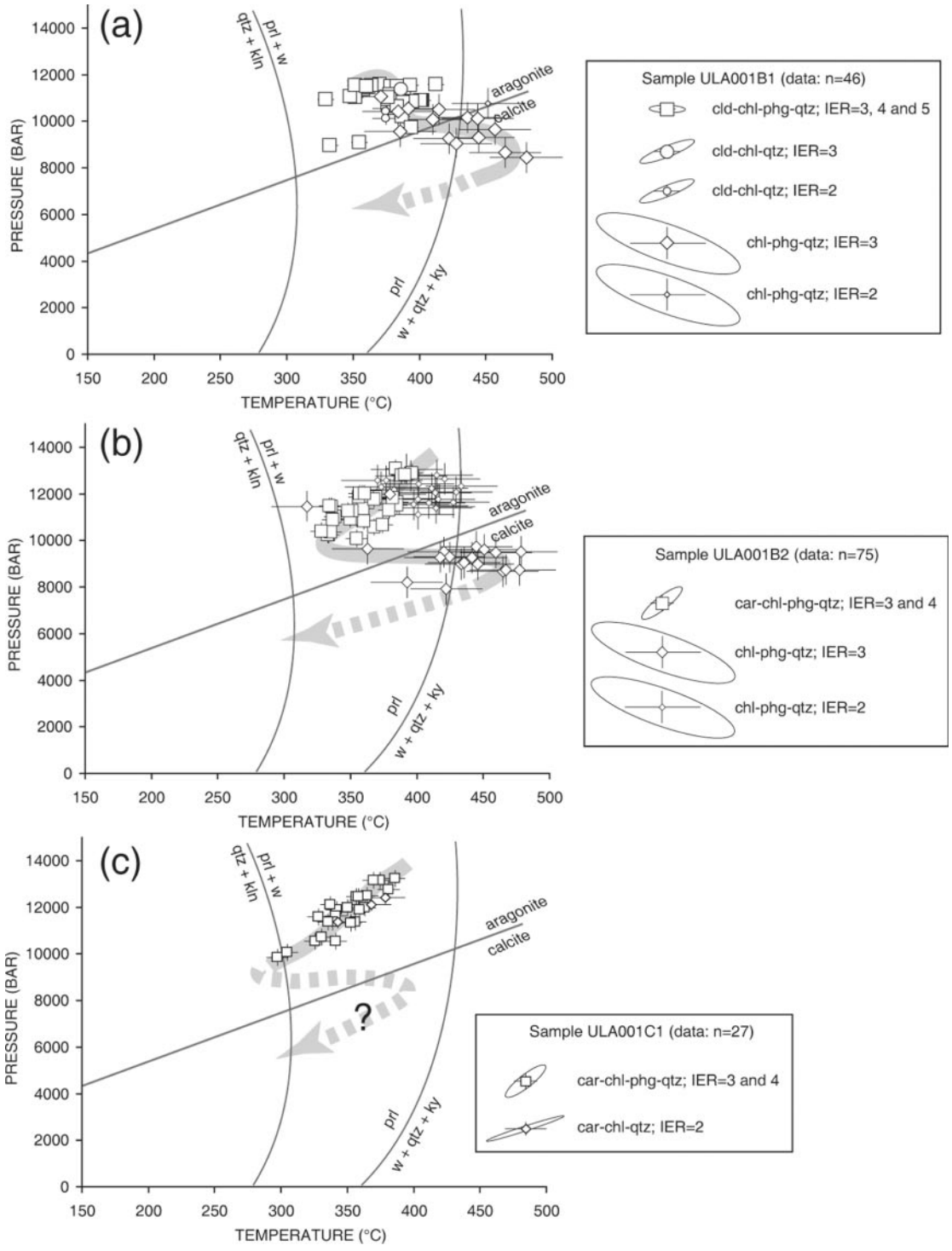

Fig. 12. *P–T* estimates for three samples (a–c) collected in the Ula region (Lycian Nappes).

(Raman Spectrometer, CNRS Villetaneuse, France), which showed only calcite spectra. No aragonite relicts have been found in these Lycian carbonate rocks. However, we performed microprobe analyses on one sample from the Rosetta limestones that was collected close to the locality of Akçakaya (GFZ microprobe (Potsdam), 15 kV, 10 nA; standard minerals: rhodonite [Mn], siderite [Fe], $CaCO_3$ [Ca], $BaAl_2Si_2O$ [Ba], dolomite [Mg],

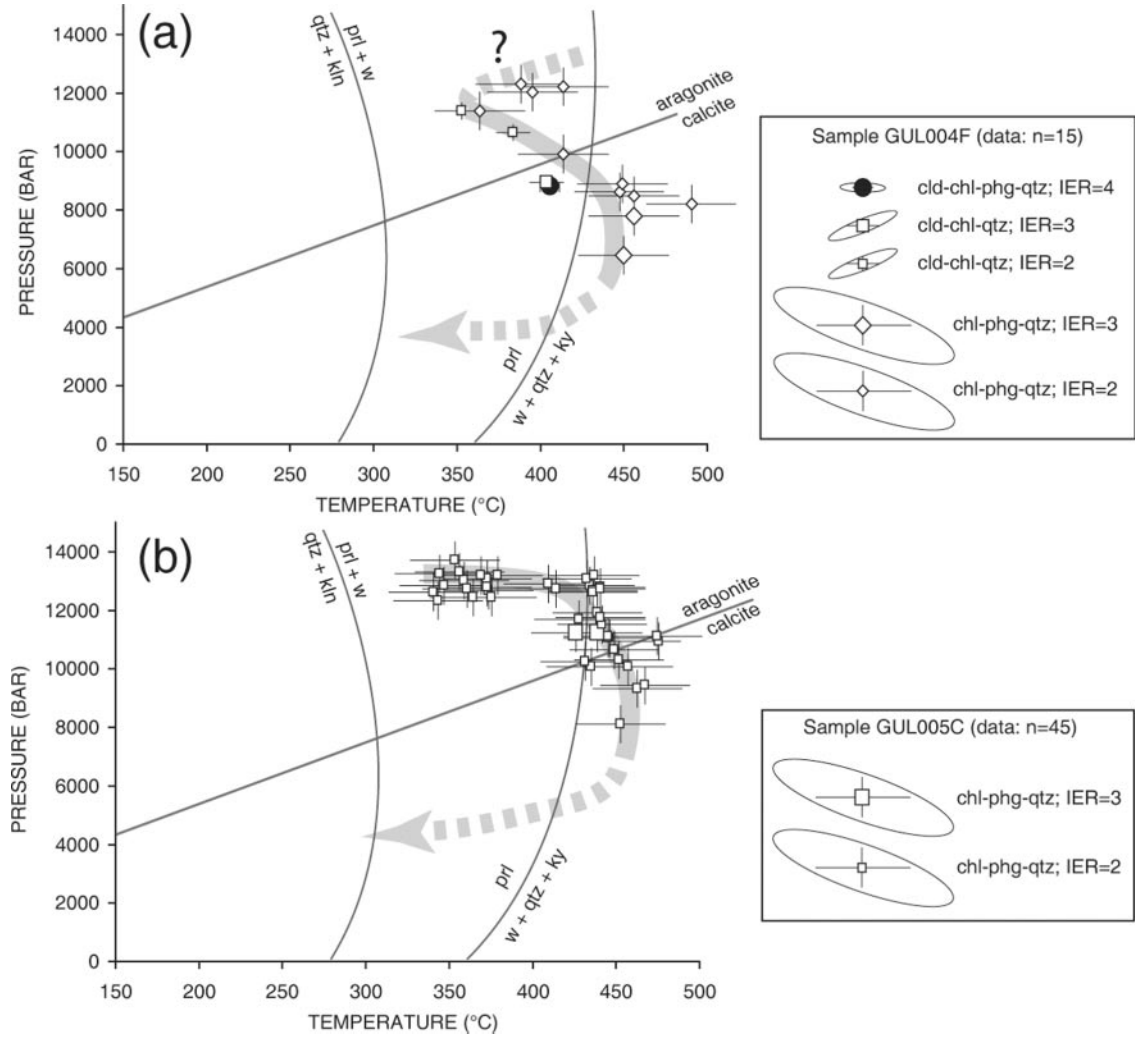

Fig. 13. *P–T* estimates for two samples (a, b) collected in the area of Güllük (Lycian Nappes).

albite [Na], celestite [Sr]; analytical spot diameter 20 μm). Analyses show very low Fe, Mn, and Mg contents (a few ppm) whereas the Sr content reaches 1500 ppm. Such values of Sr content suggest that these carbonate rocks underwent *P–T* conditions allowing growth of aragonite before its total retrogression to calcite. Similar values have already been reported for aragonite-bearing HP–LT rocks from the western Alps and the Alpujarride complex of the Betic Chain (Gillet & Goffé, 1988; Goffé *et al.*, 1989; Azañon & Goffé, 1997). We therefore propose that the underlying HP–LT rocks from the Karaova Formation might have passed into the calcite stability domain after their HP cooling path (Fig. 11). Because the original aragonite is totally retrogressed to calcite, the HP–LT rocks might have crosscut the aragonite–calcite equilibrium curve at temperatures higher than ~200°C, precluding preservation of aragonite (Gillet & Goffé, 1988).

The region of Ula. Close to the contact that separates the Lycian Nappes from the Menderes Massif, in the eastern part of the Bodrum peninsula, *P–T* estimates have been made from three samples collected at the same outcrop in the lowermost levels of the Karaova Formation (see Fig. 4 for location).

In sample ULA001B1, *P–T* estimates using several chloritoid–chlorite–phengite triplets and chloritoid–chlorite pairs from the metamorphic foliation cluster between 9 and 11·5 kbar at temperatures ranging between 330 and 400°C. Furthermore, *P–T* calculations were made with chlorite–phengite pairs that are not associated with chloritoid and are located in later textural habits (for instance, close to calcite or quartz veins that crosscut the foliation; see photomicrograph of Fig. 10b), thus allowing us to draw the directionality of the *P–T* path. The calculations show higher temperature and slightly lower pressure conditions, thus indicating that

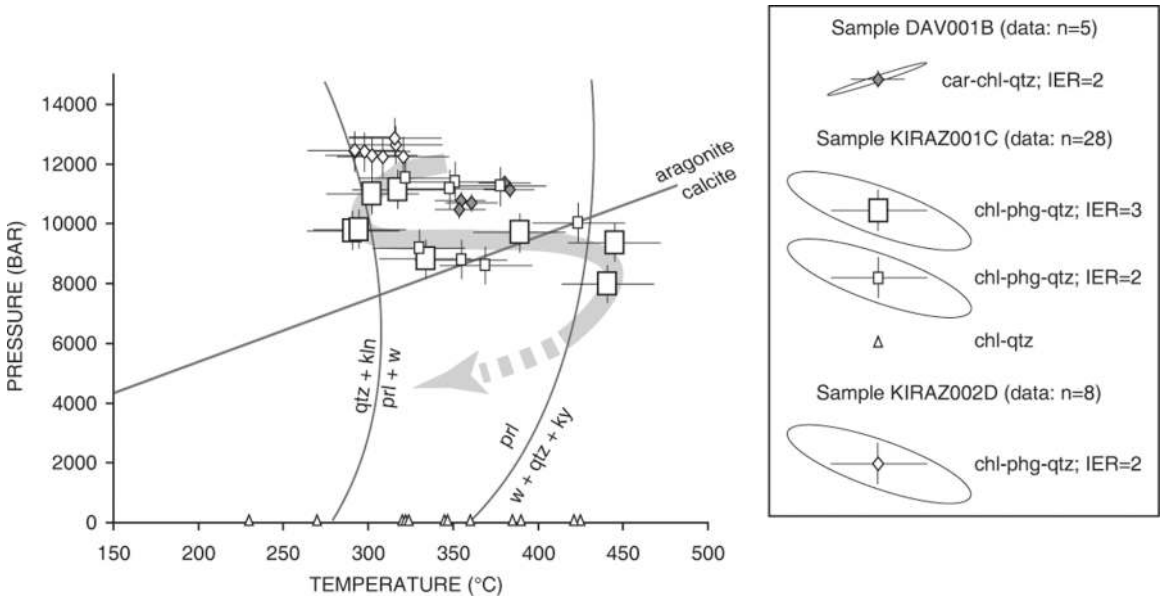

Fig. 14. *P–T* estimates for samples collected at the base of the two klippen of the Lycian Nappes located in the Dilek–Selçuk region.

temperature increased during exhumation (Fig. 12a), in contrast to the Ören-Demirciler area.

In sample ULA001B2, which contains Fe–Mg-carpholite highly retrogressed to chlorite and phengite, a similar pattern is observed. *P–T* calculations have been performed from Fe–Mg-carpholite–chlorite–phengite triplets, which indicate a HP cooling path, whereas chlorite–phengite pairs located in later textural habits reveal lower pressure and higher temperature conditions (Fig. 12b). This suggests an exhumation process in two steps: (1) a cooling exhumation path from 13–14 kbar at 400°C to 10 kbar at 320°C; (2) a thermal overprint from 320°C to 470°C at pressures of about 9–10 kbar, before late cooling and decompression.

For sample ULA001C1, in which Fe–Mg-carpholite associated with phengite and chlorite has been observed, the calculated *P–T* conditions depict the same cooling exhumation path, from 13 kbar at 380°C to 10 kbar at ~300°C. Because phengite–chlorite pairs in later habits have not been recognized within this thin section, we cannot constrain the later *P–T* path. However, the fact that sample ULA001C1 comes from the same outcrop as the two latter calls for a similar *P–T* path (Fig. 12c).

The region of Güllük. In the area of Güllük (Fig. 4), Fe–Mg-carpholite is completely retrogressed to mica and chlorite, thus pointing to an exhumation history for the rocks of this area. The foliation shows many phengite and chlorite pairs, rarely in contact with chloritoid. *P–T* conditions have been estimated from two samples (GUL004F and GUL005C). The same *P–T* trend depicted by the two samples shows a decompression path at elevated temperatures, from 12–13 kbar at 350–400°C to 7–8 kbar at 450–470°C (Fig. 13a and b). This pattern is different from that for the Ören–Demirciler or Ula regions. A HP cooling path preceding a thermal overprint such as in the samples from Ula is not observed in rocks from the region of Güllük, but is possible.

Klippen of Lycian Nappes. In Fig. 14, we have compiled all the *P–T* estimates from three samples collected in the two tectonic slices of the Lycian Nappes on the Dilek peninsula (see Fig. 5 for location). In the southern klippe (south of Tirhaköy) where fresh Fe–Mg-carpholite occurs in quartz segregations, the thin section DAV001B allowed *P–T* estimates of 10–11 kbar/350–380°C using Fe–Mg-carpholite–chlorite pairs. At the base of the northern klippe (east of Kirazlı) where chloritoid and carpholite pseudomorphs have been observed, *P–T* estimates have been made with chlorite–phengite pairs from samples KIRAZ001C and KIRAZ002D. Temperatures obtained with chlorite–quartz assemblages are also reported. The results depict a similar *P–T* trend to that of the Ula area. A cooling exhumation path from 12 kbar/350°C to 9·5–10 kbar/280°C is followed by a thermal overprint that reaches 450°C at 9 kbar.

P–T *results in the southern Menderes Massif*

In the southern Menderes Massif, *P–T* estimates have been calculated with samples from two localities where the HP–LT parageneses-bearing metaconglomerate crops out (Fig. 4).

The region of Kurudere. Near the locality of Kurudere (Fig. 4), the metamorphic peak is constrained with magnesiocarpholite–chlorite–kyanite triplets from two

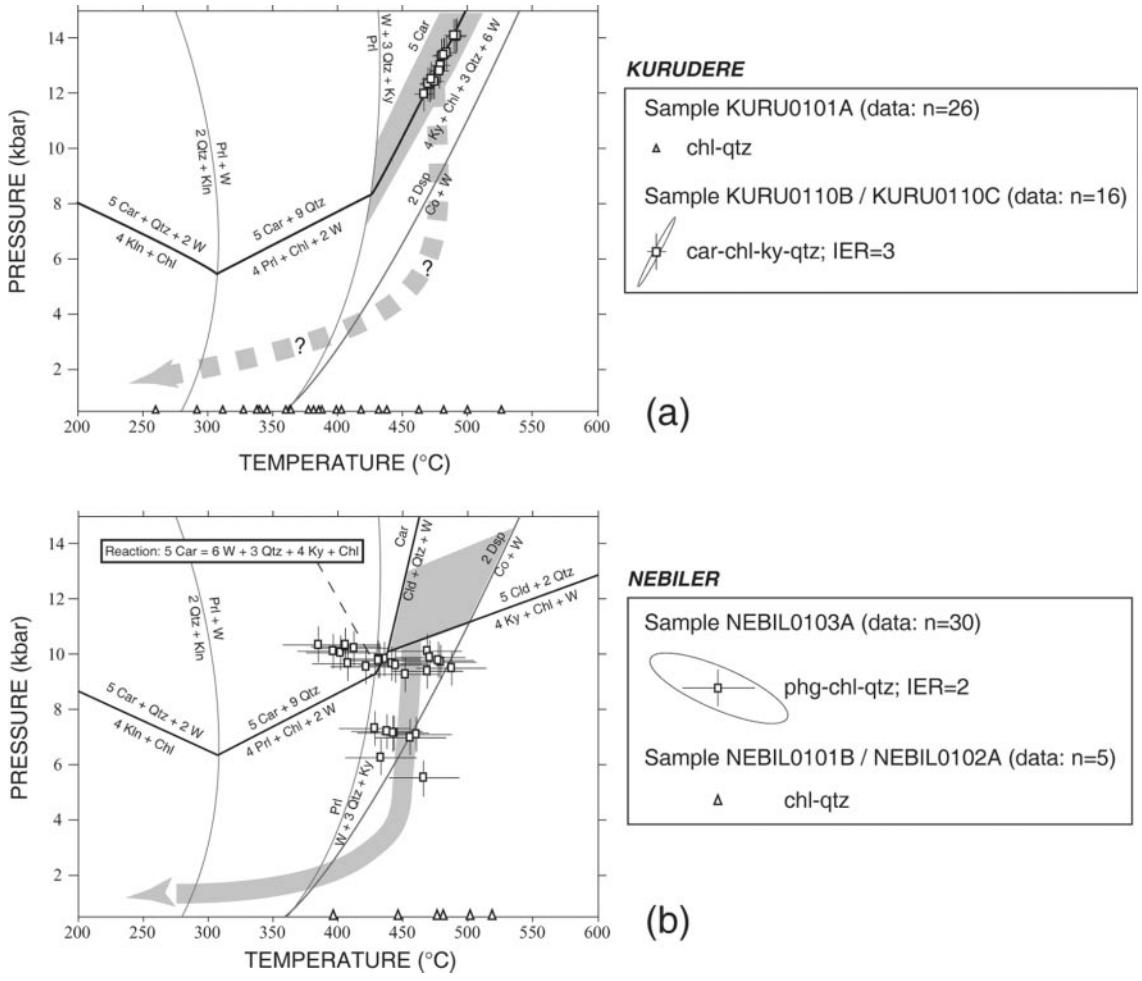

Fig. 15. *P–T* estimates for samples collected in the HP–LT metaconglomerate (Menderes Massif 'cover' series) of the Kurudere (a) and the Nebiler (b) localities. Equilibrium curves involving carpholite, chloritoid and chlorite as well as shaded domains corresponding to the HP metamorphic peak are from Rimmelé *et al.* (2003*b*).

samples (KURU0110B and KURU0110C). They indicate *P–T* conditions of 12–14 kbar and 470–500°C (Fig. 15a), higher than those of the Lycian metamorphic peak. These *P–T* conditions are similar to those already proposed by Rimmelé *et al.* (2003*b*), who also suggested a subsequent isothermal decompression during exhumation, based on the existence of corundum-bearing metasediments in the overlying rocks. In the samples from the Kurudere area, the absence of chlorite–phengite pairs did not allow us to constrain this pattern with the multi-equilibrium method. However, temperatures have been estimated using compositional variations of chlorite within sample KURU0101A, and depict a wide range between 260 and 530°C, which corresponds to their temperatures of crystallization during retrogression.

The region of Nebiler. Although retrogression of HP–LT parageneses could not be constrained in the Kurudere area with the multi-equilibrium method, phengite–chlorite pairs within the foliation of sample NEBIL0103A collected near Nebiler (Fig. 4) have been used to show the exhumation pattern of these eastern Menderes HP–LT rocks. The *P–T* estimates cluster in two domains, one located between 400 and 500°C at 9–10 kbar, and a narrower one between 420 and 470°C at pressures around 6–7 kbar (Fig. 15b). The large 95% confidence ellipse associated with the chlorite–phengite pairs as well as the low certainty of *P–T* estimates calculated with only two independent equilibrium reactions do not permit definition of a precise exhumation path for these rocks: even if the *P–T* estimates at 9–10 kbar show an isobaric increase of temperature, all the *P–T* points can be included in a single ellipse. However, the two clusters previously described show a significant pressure gap that could reasonably allow the interpretation of an isothermal decompression path passing through the two *P–T* domains. Temperatures deduced from chlorite

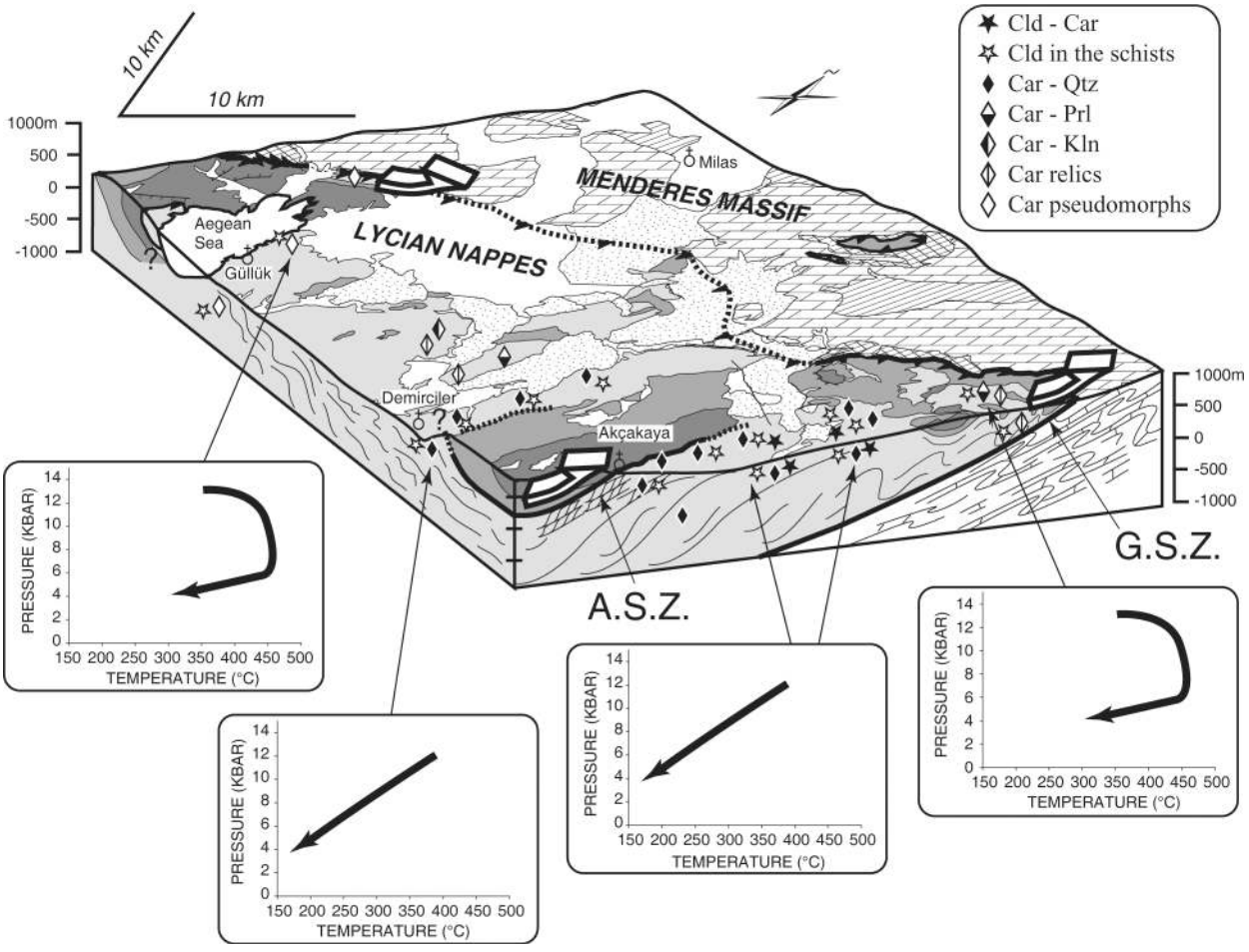

Fig. 16. Three-dimensional tectono-metamorphic diagram showing the parageneses and the different *P–T* paths in the Lycian Nappes of the Bodrum peninsula, as well as the displacements (white arrows) observed in the Akçakaya shear zone (A.S.Z.) and Gerit shear zone (G.S.Z.). Location of the block diagram and list of mineral abbreviations are shown in Fig. 4.

compositions range between 400 and 520°C, which is compatible with the *P–T* estimates obtained with chlorite–phengite pairs.

REGIONAL-SCALE INTERPRETATION AND CONCLUSIONS

HP–LT rocks from both Lycian Nappes and Menderes cover series reveal metamorphic peak conditions of about 10–12 kbar/400°C and 12–14 kbar/470–500°C, respectively, slightly higher than the minimum conditions already reported by Oberhänsli *et al.* (2001) and Rimmelé *et al.* (2003*a*, 2003*b*).

Whereas a simple isothermal decompression at about 450°C is indicated for the exhumation of HP–LT parageneses from the southern Menderes Massif, various *P–T* paths are observed in the overlying Lycian Nappes. Between Ören and Demirciler where Fe–Mg-carpholite is well preserved, all *P–T* paths depict a cooling decompression path from 12–13 kbar at 420°C to 8 kbar at 270–300°C. Similar HP cooling paths preserving Fe–Mg-carpholite have already been described for high-pressure rocks from Oman (Goffé *et al.*, 1988) and from the Valaisan domain of the Western and Central Alps (Bousquet *et al.*, 1998, 2002). Here, between Ören and Demirciler, about 10 km from the contact with the Menderes Massif, these cooling decompression paths are associated with top-to-the-NNE movements related to the Akçakaya shear zone (Fig. 16) at the top of the Karaova Formation (Rimmelé *et al.*, 2003*a*). This zone of strain localization is a local intra-nappe contact that was active during the early stages of exhumation of the HP–LT rocks, within the stability domain of Fe–Mg-carpholite.

In contrast, at the base of the Karaova Formation, close to the contact with the Menderes Massif, *P–T*

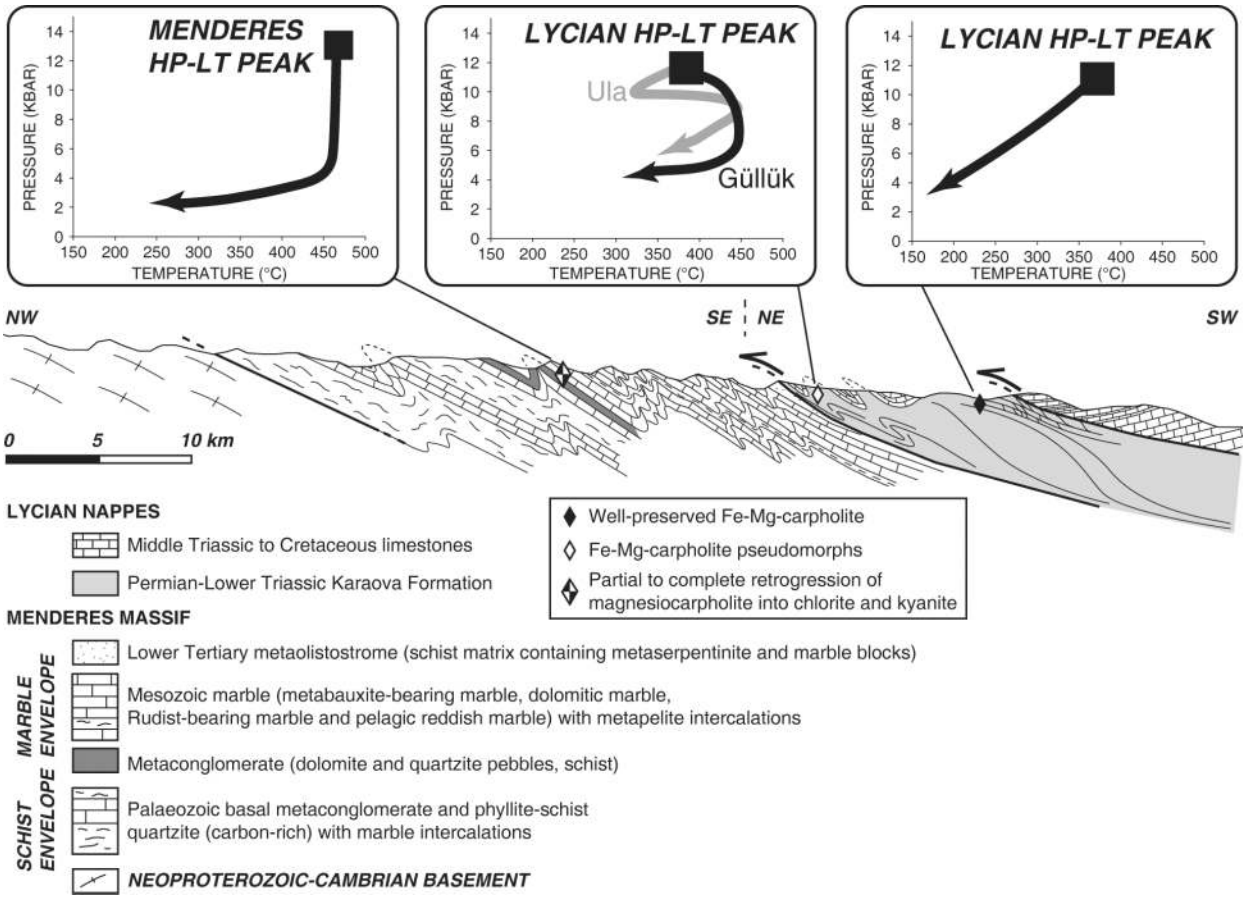

Fig. 17. Synthetic cross-section across the Lycian Thrust Sheets (Bodrum peninsula region) and the southern Menderes Massif showing the HP metamorphic peaks and retrograde *P–T* paths for both massifs. The location of the cross-section in the study area is shown in Fig. 4.

estimates revealed warmer exhumation patterns. Near Güllük, where Fe–Mg-carpholite is completely retrogressed to chlorite and phengite, *P–T* data suggest exhumation from 12 kbar/350°C to 7–8 kbar at 450–470°C. Near Ula, where a few Fe–Mg-carpholite relics have been recognized, *P–T* estimates calculated from samples collected at the same outcrop depict a retrogression path defined by cooling decompression from 13–14 kbar/400°C to 10 kbar/300°C, followed by a thermal overprint reaching 470°C at about 9 kbar. Similar trends are also observed for the exhumation path of the HP–LT rocks from the basal part of the two klippen of Lycian material located on the Dilek peninsula. For the rocks near Güllük, the first part of exhumation along a HP cooling path from 13–14 kbar/400°C to 11–12 kbar/350°C (as for HP–LT rocks from Ula) could have been erased by a stronger thermal overprint (Fig. 13). In these lowermost Lycian metasediments of the Bodrum peninsula, the pervasive deformation associated with the late warmer *P–T* paths is characterized by top-to-the-east shear senses. Approaching the contact with the Menderes Massif, deformation becomes more severe, which suggests that the Lycian–Menderes contact has been reactivated as a major shear zone (the Gerit shear zone; see Fig. 16) after the southward transport of the Lycian Nappes over the Menderes Massif (Rimmelé *et al.*, 2003*a*). This zone of strain localization facilitated late exhumation of HP parageneses under warmer conditions.

Although all these *P–T* paths have been depicted from samples collected within the same unit (the Karaova Formation), it can be argued that the Lycian metasediments recorded three distinct exhumation patterns. A single decompression–cooling path (I) is observed for the rocks located in the uppermost levels of the Karaova Formation, whereas a single decompression pattern with heating (II) or a mixture of paths (I) and (II) characterizes the exhumation of rocks located at (or towards) the base of the Karaova Formation, close to the contact with the Menderes Massif (Figs 16 and 17).

A rapid exhumation mechanism is needed to explain such a cooling decompression *P–T* path (I) for rocks

located in the uppermost lithologies of the HP–LT unit. The rocks under consideration must have returned to the surface in a cold environment along the Akçakaya shear zone, with shearing deformation allowing the HP–LT rocks to pass through roughly flat isotherms. In contrast, the rocks located at the Lycian Nappes–Menderes Massif boundary have been exhumed along the Gerit shear zone in a warmer environment, across relatively steeper isotherms to maintain the higher temperature conditions during reactivation of the contact between the Lycian Nappes and the Menderes Massif as a major shear zone. The two opposite situations are not isochronal and the exhumation processes might have occurred in a large wedge allowing, from top to base, such HP cooling and decompression with heating patterns.

ACKNOWLEDGEMENTS

We thank O. Ö. Dora for his support during our fieldwork in SW Turkey. We also thank Olivier Beyssac for performing the Raman spectrometric analyses, and Christine Fischer for the quality and number of rock thin sections. We gratefully acknowledge the Deutsche Forschungsgemeinschaft (DFG project OB80/21-2), the CNRS and the Volkswagen Stiftung for financial support. The Deutsch–Französische Hochschule (DFH) is also thanked for supporting the German–French cooperation. Daniel Bernoulli, Alan Collins and Thomas Theye are thanked for their careful and constructive reviews, which have greatly improved the manuscript.

SUPPLEMENTARY DATA

Supplementary data for this paper are available at *Journal of Petrology* online.

REFERENCES

Akkök, R. (1983). Structural and metamorphic evolution of the northern part of the Menderes massif: new data from the Derbent area and their implication for the tectonics of the massif. *Journal of Geology* **91**, 342–350.

Ashworth, J. R. & Evirgen, M. M. (1984*a*). Garnet and associated minerals in the southern margin of the Menderes Massif, southwest Turkey. *Geological Magazine* **121**(4), 323–337.

Ashworth, J. R. & Evirgen, M. M. (1984*b*). Mineral chemistry of regional chloritoid assemblages in the Chlorite Zone, Lycian Nappes, southwest Turkey. *Mineralogical Magazine* **48**, 159–165.

Avigad, D. & Garfunkel, Z. (1989). Low angle faults above and below a blueschist belt—Tinos Island, Cyclades, Greece. *Terra Nova* **1**, 182–187.

Azañon, J. M. & Goffé, B. (1997). Ferro- and magnesiocarpholite assemblages as record of high-*P*, low-*T* metamorphism in the Central Alpujarrides, Betic Cordillera (SE Spain). *European Journal of Mineralogy* **9**, 1035–1051.

Berman, R. G. (1988). Internally consistent thermodynamic data for minerals in the system Na_2O–K_2O–CaO–MgO–FeO–Fe_2O_3–Al_2O_3–SiO_2–TiO_2–H_2O–CO_2. *Journal of Petrology* **29**, 445–522.

Berman, R. G. (1991). Thermobarometry using multi-equilibrium calculations: a new technique, with petrological applications. *Canadian Mineralogist* **29**, 833–855.

Bernoulli, D., de Graciansky, P. C. & Monod, O. (1974). The extension of the Lycian Nappes (SW Turkey) into the southeastern Aegean Islands. *Eclogae Geologicae Helvetiae* **67**, 39–90.

Blake, M. C., Bonneau, M., Geyssant, J., Kienast, J. R., Lepvrier, C., Maluski, H. & Papanikolaou, D. (1981). A geological reconnaissance of the Cycladic blueschist belt, Greece. *Geological Society of America Bulletin* **92**, 247–254.

Bousquet, R., Oberhänsli, R., Goffé, B., Jolivet, L. & Vidal, O. (1998). High-pressure–low-temperature metamorphism and deformation in the Bündnerschiefer of the Engadine window: implications for the regional evolution of the eastern Central Alps. *Journal of Metamorphic Geology* **16**, 657–674.

Bousquet, R., Goffé, B., Vidal, O., Oberhänsli, R. & Patriat, M. (2002). The tectono-metamorphic history of the Valaisan domain from the Western to the Central Alps: new constraints on the evolution of the Alps. *Geological Society of America Bulletin* **114**(2), 207–225.

Bozkurt, E. (1996). Metamorphism of Palaeozoic schists in the Southern Menderes Massif: field, petrographic, textural and microstructural evidence. *Turkish Journal of Earth Sciences* **5**, 105–121.

Bozkurt, E. & Park, R. G. (1994). Southern Menderes Massif—an incipient metamorphic core complex in western Anatolia, Turkey. *Journal of the Geological Society, London* **151**, 213–216.

Bozkurt, E. & Park, R. G. (1999). The structures of the Palaeozoic schists in the southern Menderes Massif, western Turkey: a new approach to the origin of the main Menderes metamorphism and its relation to the Lycian Nappes. *Geodinamica Acta* **12**(1), 25–42.

Bozkurt, E. & Satır, M. (2000). The southern Menderes Massif (western Turkey): geochronology and exhumation history. *Geological Journal* **35**, 285–296.

Brunn, J. H., de Graciansky, P. C., Gutnic, M., Juteau, T., Lefèvre, R., Marcoux, J., Monod, O. & Poisson, A. (1970). Structures majeures et corrélations stratigraphiques dans les Taurides occidentales. *Bulletin de la Société Géologique de France* **12**(3), 515–556.

Çağlayan, A. M., Öztürk, E. M., Öztürk, Z., Sav, H. & Akat, U. (1980). Structural observations on the southern Menderes Massif (in Turkish with English summary). *Publication of the Chamber of Geological Engineers of Turkey* **10**, 9–17.

Çakmakoğlu, A. (1985). Aydin N19-d3, Marmaris O19-a2 ve Denizli M21-d3-c4, MTA report ('Paftasina ait genellestirilmis dikme kesit'). Bornova–Izmir: MTA enstitüsü Jeoloji.

Candan, O. & Dora, O. Ö. (1998). Generalized geological map of the Menderes Massif, Western Turkey. Izmir: Dokuz Eylül Universitesi Mühendislik Fakültesi.

Candan, O., Dora, O. Ö., Oberhänsli, R., Oelsner, F. & Dürr, S. (1997). Blueschist relics in the Mesozoic cover series of the Menderes Massif and correlations with Samos Island, Cyclades. *Schweizerische Mineralogische und Petrographische Mitteilungen* **77**, 95–99.

Candan, O., Dora, O. Ö., Oberhänsli, R., Çetinkaplan, M., Partzsch, J. H., Warkus, F. C. & Dürr, S. (2001). Pan-African high-pressure metamorphism in the Precambrian basement of the Menderes Massif, western Anatolia, Turkey. *International Journal of Earth Sciences* **89**(4), 793–811.

Candan, O., Çetinkaplan, M., Oberhänsli, R. & Rimmelé, G. (2002). Fe–Mg-carpholite–pyrophyllite–chloritoid-bearing Triassic metapelites from Afyon Zone, Turkey: first evidence for Alpine low-grade, high-*P*/low-*T* metamorphism. *First International Symposium of the*

Faculty of Mines (Istanbul Technical University) on Earth Sciences and Engineering, Istanbul. Journal of Conference Abstracts, 104 pp.

Çetinkaplan, M. (2002). Tertiary high pressure/low temperature metamorphism in the Mesozoic cover series of the Menderes Massif and correlation with the Cycladic Crystalline Complex. Ph.D. thesis, Dokuz Eylül Universitesi, Izmir, 323 pp.

Chopin, C., Seidel, E., Theye, T., Ferraris, G., Ivaldi, G. & Catti, M. (1992). Magnesiochloritoid, and the Fe–Mg series in the chloritoid group. *European Journal of Mineralogy* **4**, 67–76.

Collins, A. S. & Robertson, A. H. F. (1997). Lycian melange, southwestern Turkey: an emplaced Late Cretaceous accretionary complex. *Geology* **25**, 255–258.

Collins, A. S. & Robertson, A. H. F. (1998). Processes of Late Cretaceous to Late Miocene episodic thrust-sheet translation in the Lycian Taurides, SW Turkey. *Journal of the Geological Society, London* **155**, 759–772.

Collins, A. S. & Robertson, A. H. F. (1999). Evolution of the Lycian Allochthon, western Turkey, as a north-facing Late Palaeozoic to Mesozoic rift and passive continental margin. *Geological Journal* **34**, 107–138.

Collins, A. S. & Robertson, A. H. F. (2003). Kinematic evidence for Late Mesozoic–Miocene emplacement of the Lycian Allochthon over the Western Anatolide Belt, SW Turkey. *Geological Journal* **38**, 295–310.

de Graciansky, P. C. (1966). Le massif cristallin du Menderes (Taurus occidental, Asie Mineure). Un exemple possible de vieux socle granitique remobilisé. *Revue de Géographie Physique et de Géologie Dynamique, Paris (2)* **8**(4), 289–306.

de Graciansky, P. C. (1972). Recherches géologiques dans le Taurus Lycien occidental. Ph.D. thesis, Université Paris Sud, Orsay, 571 pp.

Dora, O. Ö., Candan, O., Kaya, O., Koralay, E. & Dürr, S. (2001). Revision of 'Leptite-gneisses' in the Menderes Massif: a supracrustal metasedimentary origin. *International Journal of Earth Sciences* **89**(4), 836–851.

Dürr, S. (1975). Über Alter und geotektonische Stellung des Menderes-Kristallins/SW-Anatolien und seine Aequivalente in der mittleren Aegaeis. Habilitation thesis, University of Marburg/Lahn, 106 pp.

Dürr, S., Alther, R., Keller, J., Okrusch, M. & Seidel, E. (1978). The median Aegean crystalline belt: stratigraphy, structure, metamorphism and magmatism. In: Closs, H., Roeder, D. R. & Schmidt, K. (eds) *Alps, Apennines, Hellenides*. Stuttgart: Schweizerbart, pp. 455–477.

Ersoy, S. (1993). The geological setting of the tectonic units situated on the SW Anatolia (Turkey) and their geodynamic development. *Bulletin of the Geological Society of Greece* **28**, 617–628.

Forster, M. A. & Lister, G. S. (1999). Separate episodes of eclogite and blueschist facies metamorphism in the Aegean metamorphic core complex of Ios, Cyclades, Greece. In: Mac Niocaill, C. & Ryan, P. D. (eds) *Continental Tectonics. Geological Society, London, Special Publications* **164**, 157–177.

Gautier, P. & Brun, J. P. (1994). Ductile crust exhumation and extensional detachments in the central Aegean (Cyclades and Evvia islands). *Geodinamica Acta* **7**, 57–85.

Gautier, P., Brun, J. P. & Jolivet, L. (1993). Structure and kinematics of upper Cenozoic extensional detachment on Naxos and Paros (Cyclades Islands, Greece). *Tectonics* **12**, 1180–1194.

Gessner, K. (2000). Eocene nappe tectonics and late-Alpine extension in the central Anatolide belt, western Turkey. Structure, kinematics and deformation history. Ph.D. thesis, Johannes-Gutenberg Universität Mainz, 74 pp.

Gessner, K., Piazolo, S., Güngör, T., Ring, U., Kröner, A. & Passchier, C. W. (2001*a*). Tectonic significance of the deformation patterns in granitoid rocks of the Menderes nappes, Anatolide belt, southwest Turkey. *International Journal of Earth Sciences* **89**(4), 766–780.

Gessner, K., Ring, U., Passchier, C. W. & Güngör, T. (2001*b*). How to resist subduction: evidence for large-scale out-of-sequence thrusting during Eocene collision in western Turkey. *Journal of the Geological Society, London* **158**, 769–784.

Gessner, K., Collins, A. S., Ring, U. & Güngör, T. (2004). Structural and thermal history of poly-orogenic basement: U–Pb geochronology of granitoid rocks in the southern Menderes Massif, Western Turkey. *Journal of the Geological Society, London* **161**, 93–101.

Gillet, P. & Goffé, B. (1988). On the significance of aragonite occurrences in the Western Alps. *Contributions to Mineralogy and Petrology* **99**, 70–81.

Goffé, B. & Oberhänsli, R. (1992). Ferro- and magnesiocarpholite in the 'Bündnerschiefer' of the eastern Central Alps (Grisons and Engadine window). *European Journal of Mineralogy* **4**, 835–838.

Goffé, B., Michard, A., Kienast, J. R. & Le Mer, O. (1988). A case of obduction-related high pressure, low temperature metamorphism in upper crustal nappes, Arabian continental margin, Oman: *P–T* paths and kinematic interpretation. *Tectonophysics* **151**, 363–386.

Goffé, B., Michard, A., Garcia-Duenas, V., Gonzales-Lodeiro, F., Monié, P., Campos, J., Galindo-Zaldivar, J., Jabaloy, A., Martinez-Martinez, J. M. & Simancas, F. (1989). First evidence of high pressure, low temperature metamorphism in the Alpujarride nappes, Betic Cordillera (SE Spain). *European Journal of Mineralogy* **1**, 139–142.

Güngör, T. & Erdoğan, B. (2001). Emplacement age and direction of the Lycian Nappes in the Söke–Selçuk region, western Turkey. *International Journal of Earth Sciences* **89**(4), 874–882.

Gutnic, M., Monod, O., Poisson, A. & Dumont, J. F. (1979). Géologie des Taurides occidentales (Turquie). *Mémoires de la Société Géologique de France* **137**, 1–112.

Hetzel, R. & Reischmann, T. (1996). Intrusion age of the Pan-African augen gneisses in the southern Menderes Massif and the age of cooling after Alpine ductile extensional deformation. *Geological Magazine* **133**(5), 565–572.

Hetzel, R., Romer, R. L., Candan, O. & Passchier, C. W. (1998). Geology of the Bozdağ area, central Menderes Massif, SW Turkey: Pan-African basement and Alpine deformation. *Geologische Rundschau* **87**, 394–406.

Jolivet, L. & Patriat, M. (1999). Ductile extension and the formation of the Aegean Sea. In: Durand, B., Jolivet, L., Horvàth, F. & Séranne, M. (eds) *The Mediterranean Basins: Tertiary Extension within the Alpine Orogen. Geological Society, London, Special Publications* **156**, 427–456.

Jolivet, L., Daniel, J. M., Truffert, C. & Goffé, B. (1994). Exhumation of deep crustal metamorphic rocks and crustal extension in back-arc regions. *Lithos* **33**(1/2), 3–30.

Jolivet, L., Goffé, B., Monié, P., Truffert-Luxey, C., Patriat, M. & Bonneau, M. (1996). Miocene detachment in Crete and exhumation *P–T–t* paths of high-pressure metamorphic rocks. *Tectonics* **15**(6), 1129–1153.

Jolivet, L., Rimmelé, G., Oberhänsli, R., Goffé, B. & Candan, O. (2004). Correlation of syn-orogenic tectonic and metamorphic events in the Cyclades, the Lycian Nappes and the Menderes Massif. Geodynamic implications. *Bulletin de la Société Géologique de France* **175**(3), 217–238.

Konak, N., Akdeniz, N. & Öztürk, E. M. (1987). Geology of the south of Menderes Massif. In: *Correlation of Variscan and Pre-Variscan Events of the Alpine Mediterranean Mountain Belt. Field Meeting, IGCP Project 5. Publications of the Mineral Research and Exploration Institute of Turkey*, pp. 42–53.

Lieberman, J. & Petrakakis, K. (1991). TWEEQU thermobarometry: analysis of uncertainties and application to granulites from western Alaska and Austria. *Canadian Mineralogist* **29**, 857–887.

Lips, A. L. W., Cassard, D., Sözbilir, H., Yilmaz, H. & Wijbrans, J. R. (2001). Multistage exhumation of the Menderes Massif, Western Anatolia (Turkey). *International Journal of Earth Sciences* **89**(4), 781–792.

Loos, S. & Reischmann, T. (1999). The evolution of the southern Menderes Massif in SW Turkey as revealed by zircon dating. *Journal of the Geological Society, London* **156**, 1021–1030.

Massonne, H. J. & Szpurka, Z. (1997). Thermodynamic properties of white micas on the basis of high-pressure experiments in the systems K_2O–MgO–Al_2O_3–SiO_2–H_2O. *Lithos* **41,** 229–250.

Mposkos, E. & Liati, A. (1991). Fe-carpholite in chloritoid-bearing metapelites–metasandstones of Skopelos Island, N. Sporades, Greece. *5th Congress of the Geological Society of Greece. Deltio tes Ellenikes Geologikes Etaireias (Bulletin of the Geological Society of Greece)* **25**(2), 55–66.

Mposkos, E. & Perdikatsis, V. (1984). Petrology of glaucophane metagabbros and related rocks from Samos, Aegean Islands (Greece). *Neues Jahrbuch für Mineralogie, Abhandlungen* **149**(1), 43–63.

Oberhänsli, R., Goffé, B. & Bousquet, R. (1995). Record of a HP–LT metamorphic evolution in the Valais zone: geodynamic implications. In: Lombardo, B. (ed.) *Studies on Metamorphic Rocks and Minerals of the Western Alps. A Volume in Memory of Ugo Pognante. Supplemento al Bolletino del Museo Regionale delle Scienze Naturali di Torino* **13**, 221–239.

Oberhänsli, R., Candan, O., Dora, O. Ö. & Dürr, S. H. (1997). Eclogites within the Menderes Massif/western Turkey. *Lithos* **41**, 135–150.

Oberhänsli, R., Monié, P., Candan, O., Warkus, F. C., Partzsch, J. H. & Dora, O. Ö. (1998). The age of blueschist metamorphism in the Mesozoic cover series of the Menderes Massif. *Schweizerische Mineralogische und Petrographische Mitteilungen* **78**, 309–316.

Oberhänsli, R., Partzsch, J., Candan, O. & Çetinkaplan, M. (2001). First occurrence of Fe–Mg-carpholite documenting a high-pressure metamorphism in metasediments of the Lycian Nappes, SW Turkey. *International Journal of Earth Sciences* **89**(4), 867–873.

Oberhänsli, R., Warkus, F. & Candan, O. (2002). Dating of eclogite and granulite facies relics in the Menderes Massif. In: *First International Symposium of the Faculty of Mines (Istanbul Technical University) on Earth Sciences and Engineering, Istanbul. Journal of Conference Abstracts*, 104 pp.

Okay, A. I. (1984). Distribution and characteristics of the north-west Turkish blueschists. In: Dixon, J. E. & Robertson, A. H. F. (eds) *The Geological Evolution of the Eastern Mediterranean. Geological Society, London, Special Publications* **17**, 455–466.

Okay, A. I. (1989). Geology of the Menderes Massif and the Lycian Nappes south of Denizli, western Taurides. *Bulletin of Mineral Research & Exploration (Turkey)* **109**, 37–51.

Okay, A. I. (2001). Stratigraphic and metamorphic inversions in the central Menderes Massif: a new structural model. *International Journal of Earth Sciences* **89**(4), 709–727.

Okay, A. I. & Kelley, S. P. (1994). Tectonic setting, petrology and geochronology of jadeite + glaucophane and chloritoid + glaucophane schists from north-west Turkey. *Journal of Metamorphic Geology* **12**, 455–466.

Okay, A. I., Monod, O. & Monié, P. (2002). Triassic blueschists and eclogites from northwest Turkey: vestiges of the Paleo-Tethyan subduction. *Lithos* **64**, 155–178.

Okrusch, M. & Bröcker, M. (1990). Eclogites associated with high grade blueschists in the Cyclades archipelago, Greece: a review. *European Journal of Mineralogy* **2**, 451–478.

Okrusch, M., Richter, P. & Katsikatsos, G. (1984). High-pressure rocks of Samos, Greece. In: Dixon, J. E. & Robertson, A. H. F. (eds) *The Geological Evolution of the Eastern Mediterranean. Geological Society, London, Special Publications* **17**, 529–536.

Özer, S. (1998). Rudist bearing Upper Cretaceous metamorphic sequences of the Menderes Massif (Western Turkey). *Geobios* **22**, 235–249.

Özer, S., Sözbilir, H., Özkar, I., Toker, V. & Sari, B. (2001). Stratigraphy of Upper Cretaceous–Palaeogene sequences in the southern and eastern Menderes Massif (Western Turkey). *International Journal of Earth Sciences* **89**(4), 852–866.

Özkaya, I. (1990). Origin of the allochthons in the Lycian belt, Southwest Turkey. *Tectonophysics* **177**, 367–379.

Parra, T., Vidal, O. & Agard, P. (2002*a*). A thermodynamic model for Fe–Mg dioctahedral K white micas using data from phase-equilibrium experiments and natural pelitic assemblages. *Contributions to Mineralogy and Petrology* **143**, 706–732.

Parra, T., Vidal, O. & Jolivet, L. (2002*b*). Relation between deformation and retrogression in blueschist metapelites of Tinos island (Greece) evidenced by chlorite–mica local equilibria. *Lithos* **63**, 41–66.

Partzsch, J. H., Oelsner, F. & Oberhänsli, R. (1997). The Menderes Massif, W Turkey: a complex nappe pile recording 1·0 Ga of geological history? *Terra Abstracts* **9**, 394.

Phillippson, A. (1910–1915). Reisen und Forschungen im westlichen Kleinasien. *Pet. Geogr. Mitt. Erg. Hefte der Petermanns Mitteilungen, Gotha, Justus Perthes*, pp. 167–183.

Poisson, A. (1977). Recherches géologiques dans les Taurides occidentales (Turquie). Ph.D. thesis, Université Paris Sud, Orsay, 795 pp.

Poisson, A. (1985). The extension of the Ionian trough into south-western Turkey. In: Dixon, J. E. & Robertson, A. H. F. (eds) *The Geological Evolution of the Eastern Mediterranean. Geological Society, London, Special Publications* **17**, 241–249.

Powell, R. & Holland, T. J. B. (1988). An internally consistent thermodynamic dataset with uncertainties and correlations. III. Application methods, worked examples and a computer program. *Journal of Metamorphic Geology* **6**, 173–204.

Powell, R. & Holland, T. J. B. (1994). Optimal geothermometry and geobarometry. *American Mineralogist* **79**, 120–133.

Régnier, J. L., Ring, U., Passchier, C. W., Gessner, K. & Güngör, T. (2003). Contrasting metamorphic evolution of metasedimentary rocks from the Çine and Selimiye nappes in the Anatolide belt, western Turkey. *Journal of Metamorphic Geology* **21**, 699–721.

Ridley, J. & Dixon, J. E. (1984). Reaction pathways during the progress of deformation of a blueschist metabasite: the role of chemical disequilibrium and restricted range equilibrium. *Journal of Metamorphic Geology* **2**, 115–128.

Rimmelé, G. (2003). Structural and metamorphic evolution of the Lycian Nappes and the Menderes Massif (SW Turkey): geodynamic implications and correlations with the Aegean domain. Ph.D. thesis, Universität Potsdam–Université d'Orsay-Paris XI, 243 pp.

Rimmelé, G., Jolivet, L., Oberhänsli, R. & Goffé, B. (2003*a*). Deformation history of the high-pressure Lycian Nappes and implications for tectonic evolution of SW Turkey. *Tectonics* **22**(2), 1007, doi: 10.1029/2001TC901041.

Rimmelé, G., Oberhänsli, R., Goffé, B., Jolivet, L., Candan, O. & Çetinkaplan, M. (2003*b*). First evidence of high-pressure metamorphism in the 'Cover Series' of the southern Menderes Massif. Tectonic and metamorphic implications for the evolution of SW Turkey. *Lithos* **71**, 19–46, doi: 10.1016/S0024-4937(03)00089-6.

Ring, U., Gessner, K., Güngör, T. & Passchier, C. W. (1999*a*). The Menderes Massif of western Turkey and the Cycladic Massif in the Aegean—do they really correlate? *Journal of the Geological Society, London* **156**, 3–6.

Ring, U., Laws, S. & Bernet, M. (1999*b*). Structural analysis of a complex nappe sequence and late-orogenic basins from the Aegean Island of Samos, Greece. *Journal of Structural Geology* **21**, 1575–1601.

Ring, U., Willner, A. P. & Lackmann, W. (2001). Stacking of nappes with different pressure–temperature paths: an example from the Menderes Nappes of western Turkey. *American Journal of Science* **301**, 912–944.

Satır, M. & Friedrichsen, H. (1986). The origin and evolution of the Menderes Massif, W-Turkey: a rubidium/strontium and oxygen isotope study. *Geologische Rundschau* **75**, 703–714.

Schuiling, R. D. (1962). On petrology, age and structure of the Menderes migmatite complex (SW Turkey). *Bulletin of the Institute for Mineral Research and Exploration, Turkey* **58**, 71–84.

Şengör, A. M. C. & Yılmaz, Y. (1981). Tethyan evolution of Turkey: a plate tectonic approach. *Tectonophysics* **75**, 181–241.

Şengör, A. M. C., Satır, M. & Akkök, R. (1984). Timing of tectonic events in the Menderes Massif, western Turkey: implications for tectonic evolution and evidence for Pan-African basement in Turkey. *Tectonics* **3**, 693–707.

Theye, T. & Seidel, E. (1991). Petrology of low-grade high-pressure metapelites from the External Hellenides (Crete, Peloponnese). A case study with attention to sodic minerals. *European Journal of Mineralogy* **3**, 343–366.

Theye, T., Seidel, E. & Vidal, O. (1992). Carpholite, sudoite and chloritoid in low-grade high-pressure metapelites from Crete and the Peloponnese, Greece. *European Journal of Mineralogy* **4**, 487–507.

Trotet, F. (2000). Exhumation des roches de haute pression–basse température le long d'un transect des Cyclades au Péloponnèse, implications géodynamiques. Ph.D. thesis, Université Paris Sud, Orsay, 187 pp.

Trotet, F., Jolivet, L. & Vidal, O. (2001*a*). Tectono-metamorphic evolution of Syros and Sifnos islands (Cyclades, Greece). *Tectonophysics* **338**, 179–206.

Trotet, F., Vidal, O. & Jolivet, L. (2001*b*). Exhumation of Syros and Sifnos metamorphic rocks (Cyclades, Greece). New constraints on the *P–T* paths. *European Journal of Mineralogy* **13**(5), 901–920.

Vidal, O. & Parra, T. (2000). Exhumation paths of high pressure metapelites obtained from local equilibria for chlorite–phengite assemblages. *Geological Magazine* **35**, 139–161.

Vidal, O., Goffé, B. & Theye, T. (1992). Experimental study of the stability of sudoite and magnesiocarpholite and calculation of a new petrogenetic grid for the system FeO–MgO–Al_2O_3–SiO_2–H_2O. *Journal of Metamorphic Geology* **10**, 603–614.

Vidal, O., Theye, T. & Chopin, C. (1994). Experimental study of chloritoid stability at high pressure and various fO_2 conditions. *Contributions to Mineralogy and Petrology* **118**, 256–270.

Vidal, O., Parra, T. & Trotet, F. (2001). A thermodynamic model for Fe–Mg aluminous chlorite using data from phase equilibrium experiments and natural pelitic assemblages in the 100–600°C, 1–25 kbar range. *American Journal of Science* **6**(301), 557–592.

Warkus, F. C. (2001). Untersuchungen an Hochdruckrelikten im zentralen Menderes Massiv, W Türkei. Ph.D. thesis, Universität Potsdam, 87 pp.

Whitney, D. L. & Bozkurt, E. (2002). Metamorphic history of the southern Menderes massif, western Turkey. *Geological Society of America Bulletin* **114**(7), 829–838.

Yalçin, Ü. (1987). Petrologie und Geochemie der Metabauxite SW-Anatoliens. Ph.D. thesis, Universität Bochum, 136 pp.